Infectious Disease Modelling 9 (2024) 892–925

Contents lists available at ScienceDirect

Infectious Disease Modelling

journal homepage: www.keaipublishing.com/idm

Prediction and control of cholera outbreak: Study case of Cameroon

C. Hameni Nkwayep [a, b, *], R. Glèlè Kakaï [c], S. Bowong [a, b]

[a] Laboratory of Mathematics, Department of Mathematics and Computer Science, University of Douala, PO Box 24157, Douala, Cameroon
[b] IRD, Sorbonne University, UMMISCO, F-93143, Bondy, France
[c] Biomathematics and Forest Modeling, University of Abomey-Calavi, Calavi, Benin

ARTICLE INFO

Article history:
Received 3 October 2023
Received in revised form 23 April 2024
Accepted 23 April 2024
Handling Editor: Dr Daihai He

Keywords:
Vibrio cholerae
Mathematical models
Ensemble Kalman filter
Basic reproduction number
Impulsive control

ABSTRACT

This paper deals with the problem of the prediction and control of cholera outbreak using real data of Cameroon. We first develop and analyze a deterministic model with seasonality for the cholera, the novelty of which lies in the incorporation of undetected cases. We present the basic properties of the model and compute two explicit threshold parameters $\overline{\mathcal{R}}_0$ and $\underline{\mathcal{R}}_0$ that bound the effective reproduction number $\mathcal{R}_0$, from below and above, that is $\underline{\mathcal{R}}_0 \leq \mathcal{R}_0 \leq \overline{\mathcal{R}}_0$. We prove that cholera tends to disappear when $\overline{\mathcal{R}}_0 \leq 1$, while when $\underline{\mathcal{R}}_0 > 1$, cholera persists uniformly within the population. After, assuming that the cholera transmission rates and the proportions of newly symptomatic are unknown, we develop the *EnKf* approach to estimate unmeasurable state variables and these unknown parameters using real data of cholera from 2014 to 2022 in Cameroon. We use this result to estimate the upper and lower bound of the effective reproduction number and reconstructed active asymptomatic and symptomatic cholera cases in Cameroon, and give a short-term forecasts of cholera in Cameroon until 2024. Numerical simulations show that (i) the transmission rate from free *Vibrio cholerae* in the environment is more important than the human transmission and begin to be high few week after May and in October, (ii) 90% of newly cholera infected cases that present the symptoms of cholera are not diagnosed and (iii) 60.36% of asymptomatic are detected at 14% and 86% of them recover naturally. The future trends reveals that an outbreak appeared from July to November 2023 with the number of cases reported monthly peaked in October 2023. An impulsive control strategy is incorporated in the model with the aim to avoid or prevent the cholera outbreak. In the first year of monitoring, we observed a reduction of more than 75% of incidences and the disappearance of the peaks when no control are available in Cameroon. A second monitoring of control led to a further reduction of around 60% of incidences the following year, showing how impulse control could be an effective means of eradicating cholera.

* Corresponding author. Laboratory of Mathematics, Department of Mathematics and Computer Science, University of Douala, PO Box 24157, Douala, Cameroon.
E-mail address: iverdcedric@gmail.com (C. Hameni Nkwayep).
Peer review under responsibility of KeAi Communications Co., Ltd.

https://doi.org/10.1016/j.idm.2024.04.009

1. Introduction

According to the 2019 report of World Health Organisation (WHO), diarrhoeal diseases were the fourth leading causes of death in Cameroon with 50.4 and 41.4 deaths per 100 000 population from men and women, respectively (WHOa; WHOb). Cholera is an acute diarrhoeal illness caused by infection of the intestine with *Vibrio cholerae* (*V. cholerae*). It has an indirect transmission where people can get sick when they swallow food or water contaminated with cholera bacteria and direct one comes from an adequate contact between infectious individuals (CDC; Fung, 2014). Six subsequent pandemics of cholera induced millions of death across all continents. The current (seventh) pandemic started in South Asia in 1961, reached Africa in 1971 and the Americas in 1991 (WHO Cholera). In addition, WHO continues to lament the lack of data to improve its cholera control policy. Indeed, in 2017, 71 countries provided WHO with data on cholera: 34 reported a total of 1 227 391 cases and 5654 deaths, and 37 countries reported zero cases for the year (WHOc). This would complicate global cholera time trend analyses that include the year 2017. In 2022, cholera reappeared in ten countries around the world: Haiti, Lebanon, Nepal, Kenya, Cameroon, etc … The WHO blames poverty, economic crises and wars, but also global warming. In countries that have reported cholera outbreaks in 2022, many are experiencing natural disasters such as cyclones (Mozambique, Malawi), flooding (Pakistan, Nigeria), and drought (countries in the Horn of Africa) (WHO, 2018). Also, it should be noted that climate variations are also a source of many changes in the behaviour of certain bacterial diseases. Indeed, in 2022 WHO indicated that climate change has an even more important impact on cholera outbreaks (WHOd).

The cholera disease started in Cameroon in 1971, and until 2013 main outbreaks were reported in the north in Far North and North regions and in the south of the country in the Littoral region which hosts the economic capital Douala. The country is affected by cross-border outbreaks, especially along its borders with Chad and Nigeria. In the north of Cameroon, the regions of North and Far North reported 47.3% of cholera cases between 2004 and 2013. The average case fatality rate is high ($\approx 8\%$), explained in part by poor access to health facilities and a high number of community deaths. In the south of Cameroon, the region of Littoral reported almost one third (29.6%) of cases, mainly in the city of Douala (WHO AFRO, 2018; WHO AFRO, 2019). The region of Centre containing Yaoundé reported less cases than Douala but more frequently, with cases reported in six years out of ten. There are two different seasonal patterns of cholera outbreaks in Cameroon. In fact, there is an increase of cases during the rainy season in the North (between June and October) and in the South, the number of cases usually increases from February to March (UNICEF). The cholera outbreak that started on 18 May 2018 in Cameroon is persisting (Ministry of public health, 2018; Ministry of public health). Initially, the outbreak spread from the North region of country to the Central and Littoral regions. Although the North and Littoral regions continue to report new cases, the Central region has not reported suspected cases since 27 August 2018. The cholera outbreak continue to improve. An upsurge of cholera claimed 200 lives since October 2021 in Cameroon, where 10 322 cases of the disease have been reported. More than 7 of Cameroon's 10 regions, including Littoral are affected by the epidemic (Cholera platform; Ministry of public health). One of the problems in underdeveloped or developing countries is that most people only see a doctor when they are suffering from an illness. In other words, it is the symptoms of an illness that drive them to hospital. It is therefore impossible to control asymptomatic people during an epidemic unless a massive screening campaign is launched. Also, some symptomatic prefer to be treated the old-fashioned way or with traditional pharmacopoeia, which could lead to other serious pathologies in the future (gastric problems, kidney dysfunction, etc.). Not only would it be easier to distinguish infectious cases symptomatic of cholera, but it would also be easier to diagnose them so that they could be treated with greater reassurance by the staff in charge of public health.

Saving information about phenomena is now essential in the process of anticipation and control of future phenomena. In practice, this information is not always accessible and therefore needs to be estimated using several estimation tools. With the evolution of science and the computer tools, several estimation tools have been succeeded over time: Least Squares, Monte Carlo, Optimization and Particle Filters (Cazelles, Champagne, & Dureau, 2018; Kotecha & Djuric, 2003; Tan, Cator, Ndeffo-Mbah, & Braga-Neto, 2021; Wan & van der Merwe, 2000). In 1960, R. E. Kalman published his research on a state estimation method known as the Kalman filter method (Bourgois, Roussel, & Benjelloun, 2011; Gillijns et al., 2006). Based on stochastic linear differential equations, the Kalman filter is a set of mathematical equations that gives a better estimation of states in differential system despite the imprecision of input measurements and modelling. This tool underwent several improvements with the more than more complex modelling which is reduced by strongly non-linear differential equations. The passage to the extended Kalman filter made possible the estimation of the states of non-linear problem. However, because of the linearisation of differential system, this filter gives a large margin of error between the estimated states and the exact states due to this linearisation (Bourgois et al., 2011). In 1997, the Unscented Kalman filter (*UKF*) introduced by Julier and Uhlmann (Bourgois et al., 2011; Julier & Uhlmann, 1997) has the advantage of having a better robustness for strongly non-linear systems, without requiring a significant additional computational cost in return. But, without linearisation, this filter has a cubic complexity ($0(n^3)$ where n is the dimension of the state vector) during the computation of the covariance matrix for the prediction and analysis error which makes its implementation heavy for the states with large dimension (Bourgois et al., 2011). With the non-stationarity in epidemiology and embedding time-varying parameters in stochastic models, Ensemble Kalman filter (*EnKf*) is one of the filtering that are used for the estimation values of unmeasurable states and unknown parameters even in absence of appropriate data sources (Narula, Piratla, Bansal, Azad, & Lio, 2016).

Nowadays, recurring events influence all sectors particularly in biology. For diseases influenced by pathogens liven in the environment, modelling are subject to seasonal parameters. For these systems, some parameters are not only time-varying

dependent, but known to have a periodic structure in order to take the environment factors in transmission process. Then, it is possible to use periodic functions as sinusoids to estimate the temporal behaviour of such parameters (Dietz, 1976; London & Yorke, 1973). However, it is important to illustrate a good methodology to estimate periodic time-varying parameters able to maintain known structural characteristics of evolution models. In 2016, A. Arnold and A. L. Lloyd (Andrea & Alun, 2018) gave the way by introducing a method based on *EnKf* for the estimation of a parameter which varies by intervals. Indeed, the authors consider that parameter takes several values over a period. In addition, the threshold called basic reproduction number $\mathcal{R}_0$ which gives the stability of the Disease Free Equilibrium (*DFE*) isn't explicit even if its properties do not change. To give a solution of this, N. Bacaër et al. (Bacaër & Gomes, 2009) use the average value of the periodic-transmission rate in his model to compute an estimation of $\mathcal{R}_0$ as the basic reproduction number. Early on 2022, C. H. Nkwayep et al. used the same approach to estimated $\mathcal{R}_0$ and undetected COVID-19 cases in an epidemiological model to known about incoming of news waves of COVID-19 (Hameni Nkwayep, Bowong, Tewa, & Kurths, 2020; Nkwayep, Bowong, Tsanou, Alaoui, & Kurths, 2022). But, W. Wang and X-Q. Zhao (Wang & Zhao, 2008) gave that this approach gives only the average basic reproduction number which overestimates or underestimates the infection risks in many other cases. Elsewhere, the magnitude of $\mathcal{R}_0$ is a useful indicator of both the risk of an epidemic and the effort required to control cholera disease. So, its estimation using real data should be one of the best strategies to prevent outbreak since that one could known if there are asymptomatic cases who continuous to infect susceptible even in absence of declared disease. In addition, it should be noted that *V. cholera* produced by an infectious human is more virulent than that which multiplies by mitosis in contaminated areas.

To better understand the epidemiology of cholera and to predict the impact of interventions in the future, researcher build mathematical models as tools complementary to epidemiology and statistical analysis. However, many dynamics of cholera are based on SIR models (Brauer, Shuai, & Driessche, 2013; King, Ionides, Pascual, & Bouma, 2008; Phan, Tian, & Wang, 2021; Stephen & Nkuba, 2015; Tian, Liao, & Wang, 2021). In 2013, M. C. Eisenberg et al. used rainfall in a SIR model of cholera coupled the *V. cholerae* in the environment (Eisenberg, Kujbida, Tuite, Fisman, & Tien, 2013). His work indeed underscores the need of attention from the urgent need for sewage and water management infrastructure. Even if these models take into account free bacteria *V. cholerae* in the environment, experience with COVID-19 shows that it is important to differentiate between detected and undetected cases (which in the case of cholera are the asymptomatic infectious (Isaac, 2014; King et al., 2008)). In this way, Albalawi et al. (Albalawi et al., 2023) included in 2023 quarantine individuals in their mathematical model that could determine the asymptomatic cases registered by the health authority. However, it is not sufficient according that many asymptomatic cases of cholera living among population in Africa (WHO Cholera; Deen, A Mengel, & Clemens, 2020). Early in 2023, A. Conde et al. (Conde, Dureh, & Ueranantasun, 2023) used statistical modelling to examine the occurrence and incidence rate of cholera disease in West Africa from 2012 to 2017. They developed alternative method to the traditional Poisson regression and negative binomial regression models and gave the trend of the occurrence and incidence of cholera in the sub-region. But, the model could not give forecasts about the number of undetected or asymptomatic cases that could appear in the future.

The current paper investigates the problem of the prediction and control of cholera outbreaks in Cameroon. The novelty and relevance of this work are precisely to (i) estimate the number of undetected cases of cholera and cholera asymptomatic cases, which compromise the control strategies implemented by health systems in sub-Saharan Africa, (ii) the concentration of *V. cholerae* in the environment and (iii) the value of the effective reproduction number that will give the current and future situation of this disease. We first present a deterministic model for the dynamical transmission of cholera within a human community that captures the essential biological and epidemiological features of the disease such as reported, unreported cases and the seasonality by using time-periodic cholera transmission rates. The introduction of a class cholera unreported cases is motivated by the ignorance of some patients who do not present themselves for screening after the appearance of first symptoms and prefer self medicine. We provide a theoretical analysis of the model in order to explore the role of the seasonality on the transmission of cholera within a human population. The well-posedness of the model including the boundedness of solutions and the existence of periodic disease-free solution is investigated. After the computation of the basic reproduction number $\mathcal{R}_0$ and two additional threshold parameters $\overline{\mathcal{R}}_0$ and $\underline{\mathcal{R}}_0$, we study the stability of the periodic disease-free solution. After, we use an *EnKf* approach for the reconstruction of unmeasurable state variables and unknown parameters using real data of the cholera data from January 2014 to December 2022 in Cameroon. According to the available data of cholera in Cameroon, we assume that the number of the newly reported cases of cholera are available for measurements and the cholera transmission rates, the proportion of newly symptomatic who is detected, and the detection and recovery rates of cholera asymptomatic cases are unknown parameters. Assuming that all other parameter values are known, we test the ability of the proposed *EnKf* approach to reconstruct the unmeasurable states and unknown parameters in cholera model. Since the numerical results of the test are successful, we can now use the proposed *EnKf* approach to fit the cholera model using the real data of the weekly cholera cases from January 2014 to December 2022 in Cameroon. This has permitted to estimate the number of cholera asymptomatic cases, the number of cholera unreported cases, the concentration of *V. cholerae* in the environment and the effective reproduction number (Mukandavire et al., 2011) in Cameroon during the considered period that data have been collected. We test the efficacy of the proposed *EnKf* approach to predict cholera outbreaks in Cameroon. To do so, we use the estimated parameters and state variables as the initial conditions to give the short-term forecasts of the cholera from January to April 2023 and compare the results obtained with real data in Cameroon. We found that numerical results using the proposed *EnKf* approach match well the real data of cholera in Cameroon. We are now be able to predict cholera outbreaks in Cameroon. that new wave could be observe before the end of 2023 and also 2024.

We define and implement two targeted impulsive control strategies aiming at prevent or eliminate cholera outbreaks in Cameroon. They consist in raising awareness of people to avoid contacts of people with *V. cholerae* and pouring the chlorine in areas infected by the *V. cholerae* such as water wells, traditional latrines, etc. We found that more 75% of incidences are avoided and the disappearance of the predicted peaks when no control are available in Cameroon.

The rest of the paper is organized as follows. In Section 2, we formulate and analyze a deterministic mathematical model of cholera. Section 3 is devoted to the state and parameter estimation using the *EnKf* approach. This is followed by Section 4 on concluding remarks that highlights our findings, how our work fits in the literature and how it can be extended.

2. The model framework

Herein, we give and study an epidemiological model which describes how cholera disease involves within human population.

2.1. Model construction

The description of cholera disease in most articles such as (Appoh, Apraku, Agyei, & Denteh, 2015; Chao, Longini, & Morris, 2014; Isaac, 2014; Kolaye, Damakoa, Bowong, Houe, & Békollé, 2018; Phelps et al., 2018; Amber) shows that his model could be taking two parts of population: the human individuals and the concentration of *V. cholerae* in the environment.

Here, we model the cholera disease as a infection among human population with the concentration of free *V. cholerae* in the environment.

1 Susceptible individuals S: people who are susceptible to contract cholera.
2 Asymptomatic cases C: infectious cases of cholera without any symptoms and assumed to be not registered by the health staff in charge of cholera. In fact, it is difficult in sub Saharan Africa to check a status of a disease when there are no symptoms.
3 Symptomatic detected cases I_d: infectious cases of cholera who have been registered by the health authority. It should be noted that each of these cases showed at least one symptom of cholera disease.
4 Symptomatic undetected cases I_u: infectious cases of cholera with symptoms but, are not detected due to many reasons (e.g. in remote areas, political crises, ignorance, preference to traditional medicine, …).
5 Recovered individuals R: this are infectious cases (C, I_d and I_u) who recovered from cholera disease. Here, individuals have a temporary immunity due to that the study is done during a large period of time. In fact, infection of cholera induces protection against reinfection for at least 3 years in most patients who recover (Montero et al.).
6 *V. cholerae* B: this are the concentration of free *V. cholerae* in the environment and which are responsible of indirect transmission through food or water contaminated by fluids from a person with the infection.

For direct transmission (human-human): after having an adequate contact at rate β_h with an infectious I_d, C or I_u, Susceptible individuals in S can contract the infection. Such as the Ebola disease or COVID-19, through the concentration of *V. cholerae* living in environment B and coming from the bodily fluids, dirty linens of infectious or from dirty water, Susceptible individuals can contract infection at rate β_b, that we call human-environment transmission. So, the force of infection which is the infectious probability of single Susceptible individual is

$$\lambda(t) = \beta_h(t)\frac{C(t) + \epsilon_1(I_u(t) + \epsilon_2 I_d(t))}{N(t)} + \beta_b(t)\frac{B(t)}{B(t)+K}, \tag{1}$$

where $N(t) = S(t) + I_d(t) + C(t) + I_u(t) + R(t)$ is the total number of human population, K the concentration of bacteria that infects 50% of susceptible individuals (Isaac, 2014). We assume that transmission through asymptomatic is grater than that of symptomatic. This could be attributed to the fact that infected without symptoms are free to have contact with anyone within the population which could not the case for symptomatic cases (WHO Cholera). So, $\varepsilon_1 < 1$ is the modification contacts mentioning that symptomatic couldn't infect more than asymptomatic. Also, among symptomatic, $\varepsilon_2 < 1$ presents the situation that health authorities reduce the contact with anyone and that can be the same among symptomatic undetected cases. Using the fact that one observes different seasons in each country of Sub-Saharan Africa, we could assume that the transmission rates $\beta_h(t)$ and $\beta_b(t)$ follow sinusoidal functions with

$$\beta_h(t) = \beta_{h0}\left(1 + \beta_{h1} sin\left(\frac{2\pi}{\tau_c}t\right)\right) \quad \text{and} \quad \beta_b(t) = \beta_{b0}\left(1 + \beta_{b1} sin\left(\frac{2\pi}{\tau_c}t\right)\right), \tag{2}$$

where β_{h0} and β_{b0} are the average value of β_h and β_b, respectively and $\beta_{h0}\beta_{h1}$ and $\beta_{b0}\beta_{b1}$ the amplitudes of the sinusoidal fluctuating part (Bacaër & Gomes, 2009; Chowell & Brauer, 2009; Nkwayep et al., 2022). Also, this function will use the fact that the are much contact during rainy season than other due to the increase of dirty water or to that individuals could shelter when it is raining heavily. However, depending of a local application one could choose sinusoidal function cosine at the place of sine.

Indeed, treating the symptoms of cholera with local knowledges (formal or informal), symptomatic undetected could recover at rate γ_u. Also, it is reasonable to know that after a time $1/\gamma_c$, some asymptomatic cases will develop symptoms. So, depending of the living situation, a proportion θ will be detected or will recover and move to I_d or R, respectively; at the expense of the rest $(1-\theta)$ who migrate to the class of undetected symptomatic I_u. Since that this work considers more than one period of cholera outbreak, it is right to suppose that after a certain time $1/\sigma$, some of recovered individuals return into the susceptible class. In fact, they can loss their immunity.

For this model, one supposes that the transmissions of cholera come after the inoculation of hyper-infective bacteria that can be shed by an infectious individuals. In fact, freshly shed *V. cholerae* (hyper-infectious bacteria) are 50–700 more infectious than those that were grown in-vitro (Isaac, 2014; Kolaye et al., 2018). By noting that, the infected individuals shedding *V. cholerae* in the environment, Fig. 1 shows the flow diagram that describes the different classes of cholera where the dashed arrows represent the actions between human population and the *V. cholerae* in the environment and solid arrows shows the flows between compartments.

Using the flowchart in Fig. 1, the cholera transmission model is expressed by the following system of differential equations:

$$\begin{cases} \dot{S}(t) = \Lambda + \sigma R(t) - (\lambda(t) + \mu)S(t), \\ \dot{I}_d(t) = \rho\delta\lambda(t)S(t) + \theta\alpha\gamma_c C - (\gamma_d + d_d + \mu)I_d(t), \\ \dot{C}(t) = \rho(1-\delta)\lambda(t)S(t) - (\gamma_c + \mu)C(t), \\ \dot{I}_u(t) = (1-\rho)\lambda(t)S(t) + (1-\theta)\gamma_c C - (\gamma_u + d_u + \mu)I_u(t), \\ \dot{R}(t) = \gamma_d I_d(t) + \theta(1-\alpha)\gamma_c C(t) + \gamma_u I_u(t) - (\sigma + \mu)R, \\ \dot{B}(t) = \xi_d I_d(t) + \xi_c C(t) + \xi_u I_u(t) - \mu_B B(t). \end{cases} \tag{3}$$

The biological significations and values of parameters used are reported in Table 1.

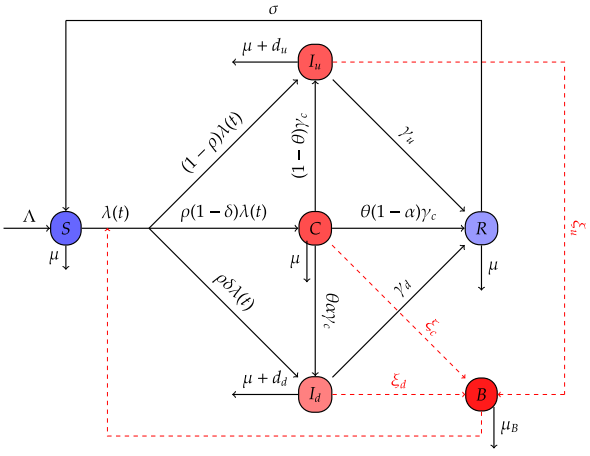

Fig. 1. Structure of the model.

Table 1
Significations and values of parameters for system (3).

Parameters	Significations	Values/Units	Refs.
Λ	Recruitment rate	229228 $ind.week^{-1}$	Bowong and Tewa (2009)
γ_d, γ_u	Recovery rate of symptomatic	1/6 $week^{-1}$	Mukandavire et al. (2011)
σ	Cholera waning-induced recovery rate	0.65/60 $week^{-1}$	Isaac (2014)
d_d, d_u	Cholera induced mortality among symptomatic	0.02 $week^{-1}$	[43, 40]
μ	Natural mortality rate in the human population	0.011 $week^{-1}$	Bowong and Tewa (2009)
μ_B	Decrease rate of concentration *V. cholerae* in the environment	6/10 $week^{-1}$	[43, 35]
ξ_d, ξ_c, ξ_u	Water contamination rates by humans	[0.01, 10] $cells.(ind.mL.week)^{-1}$	Mukandavire et al. (2011)
K	Concentration of bacteria that infects 50% of susceptible individuals	8×10^6 $cells.mL^{-1}$	[43, 35, 40]
ρ	Proportion of newly cholera cases that are detected	[0, 1]	To be estimated
δ	Proportion of detected symptomatic cases	[0, 1]	To be estimated
θ	Proportion of undetected asymptomatic cases that have been detected	[0, 1]	To be estimated
α	Proportion asymptomatic cases that are detected	[0, 1]	To be estimated
$1/\gamma_c$	Expected time to present cholera symptoms	[0, 1] $week^{-1}$	To be estimated
β_H	Cholera transmission rate from human	[0, 1] $week^{-1}$	To be estimated
β_B	Cholera transmission rate from free *V.* cholerea	[0, 1] $week^{-1}$	To be estimated
ε_1, ε_2	Modification parameters among human contacts	[0, 1]	To be estimated

2.2. Mathematical analysis

Herein, we study the biological properties and the basic reproduction number of system (3). Also, we compute two thresholds that deal with the stability of the disease free equilibrium of system (3).

2.2.1. Basic properties

Here, we study the positivity and boundedness of solutions of the system (3). Also the existence of unique maximal solution for any associated initial condition in system (3). We have the following result.

Theorem 1. *System* (3) *is a dynamical system on the biologically feasible compact domain:*

$$\Omega = \left\{ (S, I_d, C, I_u, R, B) \in \mathbb{R}^6_+,\ N \leq \frac{\Lambda}{\mu} \ \text{ and } \ B \leq \frac{\Lambda(\xi_d + \xi_c + \xi_u)}{\mu\mu_B} \right\}. \tag{4}$$

Also, for initial condition $(S(0), I_d(0), C(0), I_u(0), R(0), B(0)) \in \Omega$, *system* (3) *admits a unique maximal solution as a Cauchy problem.*

The proof of Theorem 1 is given in Appendix A.

2.2.2. Basic reproduction number

The basic reproduction number noted $\mathcal{R}_0$, a central concept in the study of the spread of infectious diseases, is the number of secondary infections caused by a single infective in a population consisting essentially only of susceptible individuals. The computation of its value needs the diseases-free equilibrium X^0 which is obtained for system (3) by setting the right part to zeros and $I_d = C = I_u = B = 0$. A simple calculation gives

$$X^0 = \left(\frac{\Lambda}{\mu}, 0, 0, 0, 0, 0 \right). \tag{5}$$

For system (3), the usual methods as in (Diekmann, Heesterbeek, & Metz, 1990; Van den Driessche & Watmough, 2002) do not work because the of time depending of transmission rates. Using the fact that system (3) is T-periodic, one uses the methodological approach of W. Wang and X-Q. Zhao (Wang & Zhao, 2008) described in the first part of Appendix B.

Define

$$X_s := \{ (I_d, C, I_u, R, B, S) \geq 0 : I_d = C = I_u = R = B = 0 \}, \tag{6}$$

the set of all disease-free states. Let

$$\mathcal{F}(t) = \begin{pmatrix} \rho\delta\lambda(t)S(t) \\ \rho(1-\delta)\lambda(t)S(t) \\ (1-\rho)\lambda(t)S(t) \\ 0 \\ 0 \\ 0 \end{pmatrix}, \quad \mathcal{V}^-(t) = \begin{pmatrix} (\gamma_d + d_d + \mu)I_d(t) \\ (\gamma_c + \mu)C(t) \\ (\gamma_u + d_u + \mu)I_u(t) \\ \mu_B B(t) \\ (\sigma + \mu)R(t) \\ \lambda(t)S(t) \end{pmatrix} \text{ and}$$

$$\mathcal{V}^+(t) = \begin{pmatrix} \theta\alpha\gamma_c C(t) \\ 0 \\ (1-\theta)\gamma_c C(t) \\ \xi_d I_d(t) + \xi_c C(t) + \xi_u I_u(t) \\ \gamma_d I_d(t) + \theta(1-\alpha)\gamma_c C(t) + \gamma_u I_u(t) \\ \Lambda - \mu S(t) + \sigma R(t) \end{pmatrix}$$

the vectors of new infections and the remaining transfer terms, respectively of system (3). Their Jacobian matrices evaluated at the *DFE* X^0 at time t > 0 are

$$F(t) = \begin{bmatrix} \rho\delta\epsilon_1\epsilon_2\beta_h(t) & \rho\delta\beta_h(t) & \rho\delta\epsilon_1\beta_h(t) & \rho\delta\dfrac{\beta_b(t)\Lambda}{K\mu} & 0 \\ \rho(1-\delta)\epsilon_1\epsilon_2\beta_h(t) & \rho(1-\delta)\beta_h(t) & \rho(1-\delta)\epsilon_1\beta_h(t) & \rho(1-\delta)\dfrac{\beta_b(t)\Lambda}{K\mu} & 0 \\ (1-\rho)\epsilon_1\epsilon_2\beta_h(t) & (1-\rho)\beta_h(t) & (1-\rho)\epsilon_1\beta_h(t) & (1-\rho)\dfrac{\beta_b(t)\Lambda}{K\mu} & 0 \\ 0 & 0 & 0 & 0 & 0 \\ 0 & 0 & 0 & 0 & 0 \end{bmatrix}$$

and

$$V(t) = \begin{bmatrix} \gamma_d + d_d + \mu & -\theta\alpha\gamma_c & 0 & 0 & 00 & \gamma_c + \mu & 0 & 0 & 0 \\ 0 & -(1-\theta)\gamma_c & \gamma_u + d_u + \mu & 0 & 0 & & & & \\ -\xi_d & -\xi_c & -\xi_u & \mu_B & 0 & & & & \\ -\gamma_d & -\theta(1-\alpha)\gamma_c & -\gamma_u & 0 & \mu + \sigma & & & & \end{bmatrix}.$$

The Jacobian matrix of non infective classes S at the *DFE* is $M(t) = -\mu$. The following steps are done to verify the properties (A1)-(A7) as defined in (Wang & Zhao, 2008) for the analyze the basic reproduction number of system (3).

1 All parameters in system (3) are non negatives. So, $\Lambda - \mu S(t) \geq 0$ in X_s and the right part of system (3) is continuous and continuously differential on $\mathbb{R} \times \mathbb{R}^6_+$. So, the functions $\mathcal{F}_i(t,x)$, $\mathcal{V}_i^+(t,x)$ and $\mathcal{V}_i^-(t,x)$ verify (A1).
2 According to Eq. (2), $\beta_h(t)$ and $\beta_b(t)$ are T-periodic. Also, $\mathcal{V}_i^+(t,.)$ and $\mathcal{V}_i^-(t,.)$ are constance since that each coefficient is constant. This implies that $\mathcal{F}_i(t,x)$, $\mathcal{V}_i^+(t,x)$ and $\mathcal{V}_i^-(t,x)$ are T-periodic in t.
3 A simple gives that vector $\mathcal{V}_i^-$ is null when $I_d = C = I_u = B = R = 0$.
4 The last coefficient of $\mathcal{F}$ is zeros.
5 In X_s, the infectious classes are zeros. So, $\mathcal{F}_i(t,x) = \mathcal{V}_i^+(t,x) = 0$ for $i = 1, 2, 3, 4$.
6 The monodromy matrix $\Phi_M(t)$ of the system $\dot{z} = -\mu z$ is $\exp(tM(t))$. A simple calculation gives

$$\Phi_M(t) = \exp(-\mu t).$$

It clear that its spectral radius of $\Phi_M(t)$ is $\exp(-\mu t)$. So, the spectral radius of $\Phi_M(t)$ at $t = T \neq 0$ is $\exp(-\mu T) < 1$. This means that the *DFE* is linearly asymptotically stable in the disease-free subspace X_s.

7 The matrix $F(t)$ is non-negative. One has:

$$-V(t) = \begin{bmatrix} -(\gamma_d + d_d + \mu) & \theta\gamma & 0 & 0 & 0 \\ 0 & -(\gamma_c + \gamma_c + \mu) & 0 & 0 & 0 \\ 0 & (1-\theta)\gamma & -(\gamma_u + d_u + \mu) & 0 & 0 \\ \xi_d & \xi_c & \xi_u & -\mu_B & 0 \\ \gamma_d & \gamma_c & \gamma_u & 0 & -(\mu + \sigma) \end{bmatrix}.$$

Since that each parameters of system (3) is positive, the matrix $-V(t)$ is cooperative. In addition, the monodromy matrix $\Phi_{-V}(t)$ is computed Appendix B (Second part), it is

$$\Phi_{-V}(T) = \tag{7}$$

$$\begin{pmatrix} e^{-(T-s)A_1} & \frac{P_1}{P_2}(e^{-(T-s)A_2}-e^{-(T-s)A_1}) & 0 & 0 & 0 \\ 0 & e^{-(T-s)A_2} & 0 & 0 & 0 \\ 0 & \frac{P_3}{P_2}(e^{-(T-s)A_2}-e^{-(T-s)A_3}) & e^{-(T-s)A_3} & 0 & 0 \\ \frac{B_2}{B_1}(e^{-(T-s)\mu_B}-e^{-(T-s)A_1}) & \Phi_1(T) & \frac{C_2}{C_1}(e^{-(T-s)A_3}-e^{-(T-s)\mu_B}) & e^{-(T-s)\mu_B} & 0 \\ \frac{B_3}{B_1}(e^{-(T-s)(\mu+\sigma)}-e^{-(T-s)A_1}) & \Phi_1(T) & \frac{C_3}{C_1}(e^{-(T-s)(\mu+\sigma)}-e^{-(T-s)A_3}) & 0 & e^{-(T-s)(\mu+\sigma)} \end{pmatrix}, \tag{7}$$

where coefficient B_1, B_2, B_3, C_1, C_2, C_3, P_1, P_2, P_3, P_4, P_5, $\Phi_1(T)$ and $\Phi_2(T)$ are computed in Appendix B (Second part).

It is simple to see that, using the fact that $e^{-(T-s)A_1}$, $e^{-(T-s)A_2}$, $e^{-(T-s)A_3}$, $e^{-(T-s)\mu_B}$ and $e^{-(T-s)(\mu+\sigma)}$ are the eigenvalues of monodromy matrix $\Phi_{-V}(T)$. So, the spectral radius of $\Phi_{-V}(T)$ is

$$\rho(\Phi_{-V}(T)) = \max\left\{e^{-(T-s)A_1}, e^{-(T-s)A_2}, e^{-(T-s)A_3}, e^{-(T-s)\mu_B}, e^{-(T-s)(\mu+\sigma)}\right\}. \tag{8}$$

Since that $T-s>0$, one has that $\rho(\Phi_{-V}(T))<1$. This concludes that the properties $(A_1)-(A_7)$ defined in (Wang & Zhao, 2008) are verified.

So, the above properties proof the Lemma 1.

Lemma 1. *The basic reproduction number $\mathcal{R}_0$ of system (3) is defined as the spectral radius of the linear operator L: $C_T \to C_T$ which is*

$$(L\varphi)(t) = \int_0^\infty \Phi(t-a)F(t-a)\varphi(t-a)da, \quad \forall t\in\mathbb{R}, \quad \varphi\in C_T, \tag{9}$$

where

$$\Phi(t-a)F(t-a)\varphi(t-a) = \begin{pmatrix} \eta_1\left(\beta_h(t-a)(C(t-a)+\epsilon_1(I_u(t-a)+\epsilon_2 I_d(t-a)))+\beta_b(t-a)\frac{\Lambda}{\mu}B(t-a)\right) \\ \eta_2\left(\beta_h(t-a)(C(t-a)+\epsilon_1(I_u(t-a)+\epsilon_2 I_d(t-a)))+\beta_b(t-a)\frac{\Lambda}{\mu}B(t-a)\right) \\ \eta_3\left(\beta_h(t-a)(C(t-a)+\epsilon_1(I_u(t-a)+\epsilon_2 I_d(t-a)))+\beta_b(t-a)\frac{\Lambda}{\mu}B(t-a)\right) \\ \eta_4\left(\beta_h(t-a)(C(t-a)+\epsilon_1(I_u(t-a)+\epsilon_2 I_d(t-a)))+\beta_b(t-a)\frac{\Lambda}{\mu}B(t-a)\right) \\ \eta_5\left(\beta_h(t-a)(C(t-a)+\epsilon_1(I_u(t-a)+\epsilon_2 I_d(t-a)))+\beta_b(t-a)\frac{\Lambda}{\mu}B(t-a)\right) \end{pmatrix},$$

with

$$\eta_1 = \rho\left(\delta e^{-aA_1}K_1 + (1-\delta)\frac{P_1}{P_2}(e^{-(T-s)A_2}-e^{-(T-s)A_1})K_2\right), \quad \eta_2 = \rho(1-\delta)e^{-(T-s)A_2}K_2,$$

$$\eta_3 = \rho(1-\delta)\frac{P_3}{P_2}(e^{-(T-s)A_2}-e^{-(T-s)A_3})K_2 + (1-\rho)e^{-(T-s)A_3}K_3,$$

$$\eta_4 = \rho\delta\frac{B_2}{B_1}(e^{-(T-s)\mu_B}-e^{-(T-s)A_1})K_1 + \rho(1-\delta)\Phi_1(T)K_2 + (1-\rho)\frac{C_2}{C_1}(e^{-(T-s)A_3}-e^{-(T-s)\mu_B})K_3,$$

$$\eta_5 = \rho\delta\frac{B_3}{B_1}(e^{-(T-s)(\mu+\sigma)}-e^{-(T-s)A_1})\rho(1-\delta)\Phi_2(T)K_2 + (1-\rho)\frac{C_3}{C_1}(e^{-(T-s)(\mu+\sigma)}-e^{-(T-s)A_3})K_3$$

and C_T is the set of T-periodic continuous functions on $\mathbb{R}$.

$\mathcal{R}_0 = \rho(L)$ can not be computed, but, his value compared to the unity is the same as the comparison with the spectral radius of the monodromy matrix of $\Phi_{F-V}(T)$ and the unity. So, the following theorem is proof (Bacaër & Guernaoui, 2006; Wang & Zhao, 2008).

Theorem 2. *The basic reproduction number $\mathcal{R}_0$ verifies the following statements:*

(i) $\mathcal{R}_0 = 1$ *if and only if* $\rho(\Phi_{F-V}(T)) = 1$.
(ii) $\mathcal{R}_0 > 1$ *if and only if* $\rho(\Phi_{F-V}(T)) > 1$.
(iii) $\mathcal{R}_0 < 1$ *if and only if* $\rho(\Phi_{F-V}(T)) < 1$.

Thus, X^0 is local asymptotically stable if $\mathcal{R}_0 < 1$ and unstable if $\mathcal{R}_0 \geq 1$.

Even if we didn't quantified $\mathcal{R}_0$, it is important to quantify thresholds that can insure the stability of the *DFE* X^0. To do this, we use the bounded transmission rates and the some states in system (3). It is:

$$\begin{array}{l}\beta_{hmin} = \beta_{h0}(1-\beta_{h1}) \leq \beta_h(t) \leq \beta_{h0}(1+\beta_{h1}) = \beta_{hmax},\\ \beta_{bmin} = \beta_{b0}(1-\beta_{b1}) \leq \beta_B(t) \leq \beta_{b0}(1+\beta_{b1}) = \beta_{bmax},\end{array} \qquad \text{for all } t \geq 0 \tag{10}$$

and

$$S(t) \leq N(t),\ S(t) \leq \frac{\Lambda}{\mu} \text{ and } (K + B(t))^{-1} \leq K^{-1}, \qquad \text{for all} t \geq 0. \tag{11}$$

This implies that, the system (3) is bounded at its left by

$$\begin{cases}\dot{\underline{S}}(t) = \Lambda + \sigma\underline{R}(t) - (\underline{\lambda}(t) + \mu)\underline{S}(t),\\ \dot{\underline{I}}_d(t) = \rho\delta\underline{\lambda}(t)\underline{S}(t) + \theta\alpha\gamma_c\underline{C} - (\gamma_d + d_d + \mu)\underline{I}_d(t),\\ \dot{\underline{C}}(t) = \rho(1-\delta)\underline{\lambda}(t)\underline{S}(t) - (\gamma_c + \mu)\underline{C}(t),\\ \dot{\underline{I}}_u(t) = (1-\rho)\underline{\lambda}(t)\underline{S}(t) + (1-\theta)\gamma_c\underline{C} - (\gamma_u + d_u + \mu)\underline{I}_u(t),\\ \dot{\underline{R}}(t) = \gamma_d\underline{I}_d(t) + \theta(1-\alpha)\gamma_c\underline{C}(t) + \gamma_u\underline{I}_u(t) - (\sigma + \mu)\underline{R},\\ \dot{\underline{B}}(t) = \xi_d\underline{I}_d(t) + \xi_c\underline{C}(t) + \xi_u\underline{I}_u(t) - \mu_B\underline{B}(t),\end{cases} \tag{12}$$

and at the right with

$$\begin{cases}\dot{\overline{S}}(t) = \Lambda - \mu\overline{S}(t) + \sigma\overline{R}(t) - \left[\beta_{hmax}(\epsilon_1\epsilon_2\overline{I}_d(t) + \overline{C}(t) + \epsilon_2\overline{I}_u(t)) + \dfrac{\beta_{bmax}\Lambda}{K\mu}\overline{B}(t)\right],\\ \dot{\overline{I}}_d(t) = \rho\delta\left[\beta_{hmax}(\epsilon_1\epsilon_2\overline{I}_d(t) + \overline{C}(t) + \epsilon_2\overline{I}_u(t)) + \dfrac{\beta_{bmax}\Lambda}{K\mu}\overline{B}(t)\right] + \theta\alpha\gamma_c\overline{C} - (\gamma_d + d_d + \mu)\overline{I}_d(t),\\ \dot{\overline{C}}(t) = \rho(1-\delta)\left[\beta_{hmax}(\epsilon_1\epsilon_2\overline{I}_d(t) + \overline{C}(t) + \epsilon_2\overline{I}_u(t)) + \dfrac{\beta_{bmax}\Lambda}{K\mu}\overline{B}(t)\right] - (\gamma_c + \mu)\overline{C}(t),\\ \dot{\overline{I}}_u(t) = (1-\rho)\left[\beta_{hmax}(\epsilon_1\epsilon_2\overline{I}_d(t) + \overline{C}(t) + \epsilon_2\overline{I}_u(t)) + \dfrac{\beta_{bmax}\Lambda}{K\mu}\overline{B}(t)\right] + (1-\theta)\gamma_c\overline{C} - (\gamma_u + d_u + \mu)\overline{I}_u(t),\\ \dot{\overline{R}}(t) = \gamma_d\overline{I}_d(t) + \theta(1-\alpha)\gamma_c\overline{C}(t) + \gamma_u\overline{I}_u(t) - (\sigma + \mu)\overline{R},\\ \dot{\overline{B}}(t) = \xi_d\overline{I}_d(t) + \xi_c\overline{C}(t) + \xi_u\overline{I}_u(t) - \mu_B\overline{B}(t).\end{cases} \tag{13}$$

Note that, the *DFE* of systems (12) and (13) is X^0. So, using the comparison approach of dynamical system (Burlando, 1991; Marek, 1970; Signing, Tsanou, Bowong, & Lubuma, 2010), the stability of X^0 for system (13) implies thet stability for system (3). Also, the instability of X^0 for system (12) implies the instability for systeml (3).

Since the parameters in systems (12) and (13) are all constants, the method of Van Den Driessche and Watmough's method (Van den Driessche & Watmough, 2002) is used to compute theirs basic reproduction numbers $\underline{\mathcal{R}}_0$ and $\overline{\mathcal{R}}_0$, respectively, as shown in the third part of Appendix B given by

$$\overline{\mathcal{R}}_0 = \overline{\mathcal{R}}_{0d} + \overline{\mathcal{R}}_{0C} + \overline{\mathcal{R}}_{0u} + \overline{\mathcal{R}}_{0B}, \tag{14}$$

and

$$\underline{\mathcal{R}}_0 = \underline{\mathcal{R}}_{0d} + \underline{\mathcal{R}}_{0C} + \underline{\mathcal{R}}_{0u} + \underline{\mathcal{R}}_{0B}. \tag{15}$$

$$
\begin{aligned}
\overline{\mathcal{R}}_{0d} &= \frac{\epsilon_1\epsilon_2\rho\beta_{h0}(1+\beta_{h1})}{A_1}\left(\delta+\frac{(1-\delta)\theta\alpha\gamma_c}{A_2}\right),\ \underline{\mathcal{R}}_{0C}=\frac{\rho(1-\delta)\beta_{h0}(1+\beta_{h1})}{A_2},\\
\overline{\mathcal{R}}_{0u} &= \frac{\epsilon_1\beta_{h0}(1+\beta_{h1})}{A_3}\left(1-\rho+\frac{\rho(1-\delta)(1-\theta)\gamma_c}{A_2}\right),\\
\overline{\mathcal{R}}_{0B} &= \frac{\beta_{b0}(1+\beta_{b1})\Lambda}{K\mu\mu_B}\left[\left(\delta+\frac{(1-\delta)\theta\alpha\gamma_c}{A_2}\right)\frac{\rho\xi_d}{A_1}+\frac{\rho(1-\delta)\xi_c}{A_2}+\left(1-\rho+\frac{\rho(1-\delta)(1-\theta)\gamma_c}{A_2}\right)\frac{\xi_u}{A_3}\right],\\
\underline{\mathcal{R}}_{0d} &= \frac{\epsilon_1\epsilon_2\rho\beta_{h0}(1-\beta_{h1})}{A_1}\left(\delta+\frac{(1-\delta)\theta\alpha\gamma_c}{A_2}\right),\quad \underline{\mathcal{R}}_{0C}=\frac{\rho(1-\delta)\beta_{h0}(1-\beta_{h1})}{A_2},\\
\underline{\mathcal{R}}_{0u} &= \frac{\epsilon_1\beta_{h0}(1-\beta_{h1})}{A_3}\left(1-\rho+\frac{\rho(1-\delta)(1-\theta)\gamma_c}{A_2}\right)\quad \text{and}\\
\underline{\mathcal{R}}_{0B} &= \frac{\beta_{b0}(1-\beta_{b1})\Lambda}{K\mu\mu_B}\left[\left(\delta+\frac{(1-\delta)\theta\alpha\gamma_c}{A_2}\right)\frac{\rho\xi_d}{A_1}+\frac{\rho(1-\delta)\xi_c}{A_2}+\left(1-\rho+\frac{\rho(1-\delta)(1-\theta)\gamma_c}{A_2}\right)\frac{\xi_u}{A_3}\right],\\
A_1 &= \gamma_d+d_d+\mu,\quad A_2=\gamma_c+\mu\quad \text{and}\quad A_3=\gamma_u+d_u+\mu.
\end{aligned}
$$

Since the stability of *DFE* X^0 for system (3), one can deduce via the istability for systems (12) and (13), the following lemma is straightforward.

Lemma 2. *The basic reproduction number* $\mathcal{R}_0$ *of system* (3) *verifies the following statements:*

(a) $\mathcal{R}_0<1$ *if* $\overline{\mathcal{R}}_0<1$.
(b) $\mathcal{R}_0\geq 1$ *if* $\underline{\mathcal{R}}_0\geq 1$.

Remark 1. *The threshold compared to the unity which gives the global asymptomatic stability of* X^0 *for systems* (12) *and* (13).

The instability of X^0 for system (12) is the consequence of the results of the method of van Den Driessche and Watmough's (Van den Driessche & Watmough, 2002), while the global asymptotic stability of the DFE for the upper system (13) is deduced from system (13). Thus, we combine Lemma 2 and the comparison principle (Burlando, 1991; Signing et al., 2010) to prove the global asymptotic stability of the *DFE*. We have obtained the following result.

Theorem 3. *System* (3) *has a DFE* X^0 *that is globally asymptotically stable if* $\overline{\mathcal{R}}_0<1$ *and unstable when* $\underline{\mathcal{R}}_0\geq 1$.

The thresholds $\underline{\mathcal{R}}_0$ and $\overline{\mathcal{R}}_0$ play an important role on the cholera outbreak within a human community. Indeed, if $\overline{\mathcal{R}}_0<1$, the cholera epidemic will disappear, while if $\underline{\mathcal{R}}_0\geq 1$, cholera tends to persist within a human community. The epidemiological consequence of the global asymptotic stability of the *DFE* is that the community-wide implementation of control interventions that can bring (and maintain) $\overline{\mathcal{R}}_0$ to a value less than unity will lead to an effective control (or elimination) of cholera within a human community. Thus, to avoid or prevent cholera outbreaks, we need to estimate the t thresholds $\underline{\mathcal{R}}_0$ and $\overline{\mathcal{R}}_0$ which contain the bounds of transmission rates that cannot be measure directly. However, estimating these thresholds alone would be not sufficient, since it is also important to estimate the number of cholera undetected and asymptomatic cases and the concentration of *V. cholerae* in the environment. The aim of the next section is to propose an estimation technique based on an *EnKf* approach for the estimation of unmeasurable state variables and unknown parameters in system (3) using real data of Cameroon. This will permit to predict cholera outbreaks in Cameroon.

3. State and parameter estimation

Herein, we present how system (3) should be transform into a problem that one can use *EnKf* developed in Appendix C to estimate the state variables and unknown parameters of system (3).

3.1. Problem statement

To estimate the states of system (3) with the above design, it is important that one models a function for the available observations. So, the estimation of each parameter and states in that function could be estimated with a good precision.

Currently, the available data of cholera is reported each week during a year. In system (3), the newly reported cases of cholera are some asymptomatic who begin to present symptoms $\alpha\theta\gamma_c C(t)$ and the newly susceptible who directly show the symptoms of cholera and have been declared by the public health staff which are $\rho\delta\lambda(t)S(t)$. Thus, the observation of system (3) is $\mathcal{H}(t)=\rho\delta\lambda(t)S(t)+\alpha\theta\gamma_c C(t)$. To take into account the fact this observation could be not perfect, the measurable data is then written as follows:

$$\mathcal{Y}_t = \mathcal{H}(t) + \vartheta_t, \tag{16}$$

where $\vartheta_t \in \mathbb{R}$ is the white noise that is assumed to be a Gaussian distribution with deviation Z_t.

To give the best value of function $\mathcal{H}(t)$ which approaches the data at each time $t \geq 0$, his parameters need to be estimated. So, one assumes β_{h0}, β_{h1}, β_{b0}, β_{b1}, ε_1, ε_2, ρ, δ, θ, α and γ_c to be unknown in system (3). Indeed, these parameters can be estimated in system (3) using the *EnKf* method since that observed function $\mathcal{H}(t)$ in Eq. (16) depends on these parameters. Thus, the unknown parameters at time t are grouped in the following vector:

$$\psi_t = (\beta_{h0,t}, \beta_{b1,t}, \beta_{b0,t}, \beta_{b1,t}, \epsilon_{1,t}, \epsilon_{2,t}, \rho_t, \delta_t, \theta_t, \alpha_t, \gamma_{c,t})^T,$$

that we write in a simple state space model following a Markov process:

$$\psi_{t+1} = \psi_t + \chi_t, \tag{17}$$

where χ_t is the uncertainty at time t given by a Gaussian white noise in $\mathbb{R}^{10}$ with standard deviations R_t. In fact, χ_t can be interpreted as the behaviour changes influence on the transmission rates that grow or fall beyond certain limits 0 and 1. However, the above formulation is for the estimating during the first period T. In fact, each new report on cholera in sub-Saharan Africa always includes a comparative study of the situation during the same period of the previous year (Ministry of public health). So, this aspect is taken into account in the design of unknown parameters ψ_t. One considers that the next value ψ_t of unknown parameters depends on her previous value at time $t - kT$. It is

$$\psi_t = \psi_{t-kT} + \chi_t. \tag{18}$$

After, one uses the estimates parameters ψ_t at each time $t \geq 0$ to estimate the following unknown rates:

(a) The transmission rates $\beta_i(t) = \beta_{i0,t}\left(1 + \beta_{i1,t}\sin\left(\frac{2\pi}{T}t\right)\right), \quad i \in \{h, b\}$,
(b) Proportion of newly symptomatic detected $\omega = \rho\delta$,
(c) Detected rate of Asymptomatic $\eta = \theta\alpha\gamma_c$,
(d) Recovery rate of Asymptomatic $\varphi = \theta(1 - \alpha)\gamma_c$.

In additional, we simulate system (3) using the fourth order Runge-Kutta method with the function $f(x_t, \psi_t)$ as the approximated value of x_{t+1}. Since each variable of system (3) follows a Markov process (Bourgois et al., 2011; Tan et al., 2021), we use the following discrete model:

$$x_{t+1} = f(x_t, \psi_t) + \zeta_t, \tag{19}$$

where ζ_t is the incertitude at time t of the discretization (error) that is assumed to be a white noise process with the covariance matrix Q_t which appreciates the estimation to the exact value of the state variable $x(t) \equiv x_t = (S(t), I_d(t), C(t), I_u(t), R(t), B(t))^T$.

Combining equations (16)–(19), the problem of estimation is to find the state variable x_t and parameters χ_t so that the model

$$\begin{cases} x_{t+1} & = f(x_t, \psi_t) + \zeta_t, \\ \mathcal{Y}_t & = \mathcal{H}(t) + \vartheta_t, \\ \psi_{t+1} & = \psi_t + \chi_t, \quad \text{if } t \in [0, T], \\ \psi_t & = \psi_{t-kT} + \chi_t, \quad \text{if } t \in [kT, (k+1)T], \end{cases} \tag{20}$$

gives the best approximation of available data of cholera.

In the sequel, we will apply the above method using a toy model and after by using data of the current epidemic of cholera in Cameroon. Indeed, it is important to note that the approach used in this work (described in Appendix C) (Andrea & Alun, 2018) is difference for the one used in an early work on COVID-19 disease with seasonal transmission(Nkwayep, Bah, Tsanou, & Bowong, 2023). In fact, each parameter in this work is supposed to be seasonal (as shows Eqs. (17) and (18)) while in Ref. (Nkwayep et al., 2023), parameters have only the form described in Eq. (17). So, the thresholds in Theorem 3 that we'll estimate at each time represent the effective reproduction.

3.2. Reconstruction of the dynamics of the cholera model with toy model

Herein, we show the ability of the proposed estimation method to reconstruct the trajectories of all state variables and estimate some parameters of cholera using system (3). The toy model aims to test the *EnKf* algorithm on simulated infectious disease data. The role of the toy model is to test the ability of the *EnKf* algorithm to reconstruct the trajectories of all state variables and estimate some parameters of cholera in system (3). To do this, we proceed as follows:

(i) we simulate system (3) considering that the rates β_{h0}, β_{h1}, β_{b0}, β_{b1}, ε_1, ε_2, ρ, δ, θ, α_t and γ_c are known.
(ii) The simulated states are used to compute the incidence (observations $\mathcal{Y}(t) = \rho\delta\lambda(t)S(t) + \alpha\theta\gamma_c C(t)$) of cholera over 2 years (105 week) with period $\tau = 52$.
(iii) We use the *EnKf* framework to estimate the state variables and parameters of the simulated model and compare the posterior distributions of the parameters with the given values.

The illustration is done by taking 12 components of each parameter for instance $(\beta_{h0}, \beta_{h1}) = \{(\beta_{h0,1}, \beta_{h1,1}), (\beta_{h0,2}, \beta_{h1,2}), \ldots, (\beta_{h0,12}, \beta_{h1,12})\}$ corresponding to monthly observations of incidence cases (new infected cases) per period.

Figs. 2 and 3 present the comparison between the exact values (blue line) and estimation values (magenta line) of state variables and transmission rates of system (3) with initial condition $X_0 = (16\,800{,}100{,}300{,}150{,}200{,}10\,000)^T$. The deviation used are: $Q_t = 2.5 \times diag(200, 100, 100, 1000)$, $R_t = 10^{-5} \times diag(1, 1, 1, 1)$ and $Z_t = 1.5$. The exact values of rates are $\beta_{h0} = 0.2$, $\beta_{h1} = 0.09$, $\beta_{b0} = 0.511$, $\beta_{b1} = 0.095$, $\varepsilon_1 = 0.5$, $\varepsilon_2 = 0.5$, $\rho = 0.3$, $\delta = 1/3$, $\theta = 1/12$, $\alpha = 0.02$ and $\gamma_c = 1/6$. It is important to note that these values are not necessary true, they are for the ability test. All other parameters are reported in Table 1.It illustrates that the reconstruction of the incidences and parameters follow the exact values. In fact, the state estimations are in perfect agreement with the values used to generate the observations (see Fig. 2-(a)–(f)) and the estimation process correctly

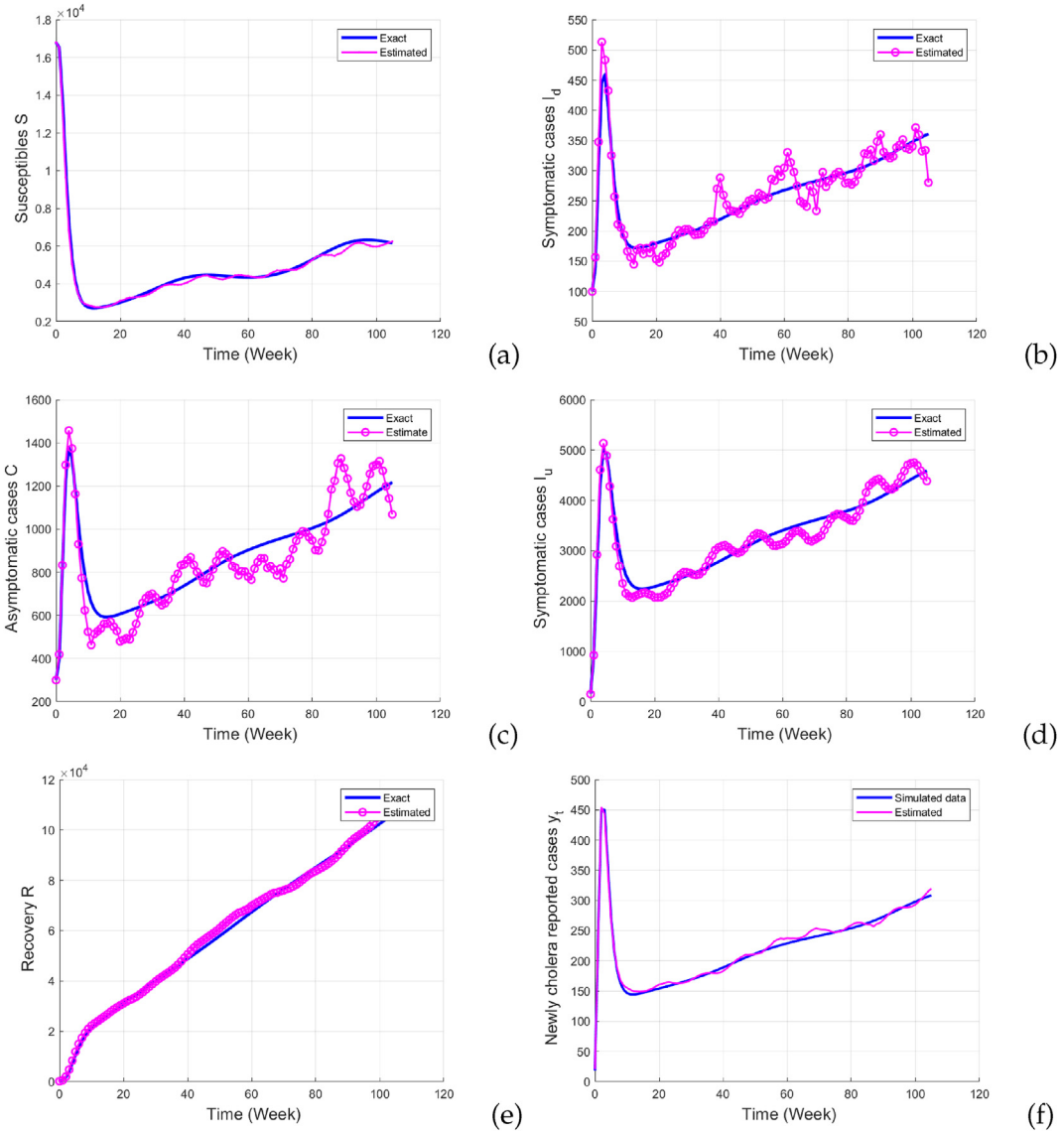

Fig. 2. Comparison between the exact value (blue line) and the estimated value (magenta line) using a toy model. (a) Susceptible individuals S, (b) Symptomatic detected I_d, (c) Asymptomatic C, (d) Symptomatic undetected I_u, (e) Recovered individuals R and (f) Newly cholera reported cases $\mathcal{Y}_t$.

converged (see Fig. 2-(e)). Concerning the estimation of transmission rates β_h and β_b, one notes a perfect fitting between exact values and estimations. The results in Figs. 2 and 3 show that one can use real data of new reported cases to estimate the unmeasurable states and unknown parameters.

In the next subsection, we apply the design of *EnKf* constructed above to display the situations of cholera disease in Cameroon.

3.3. Parameters and states estimation of cholera in Cameroon

Here, we use the estimation method developed in the previous section can estimate the unmeasurable state variables and unknown parameters of cholera using real data available in Cameroon.

To estimate the unmeasurable state variables and unknown parameters for the cholera outbreak in Cameroon using system (3), we used the weekly data of cholera cases reported by Cameroon Ministry of Public Health for the period from January 2014 to December 2022 (Ministry of public health, 2018; Ministry of public health). Thus, we exactly use 469 data for estimation in the case of cholera. These data are fitted in the *EnKf* constructed above. We used the demographic of Cameroon in 2014 and epidemiological parameter values of cholera (Bowong & Tewa, 2009; Isaac, 2014; Kolaye et al., 2018; Mukandavire et al., 2011) reported in Table 1 as known parameters value and set the initial state for system (3) in Cameroon. It's

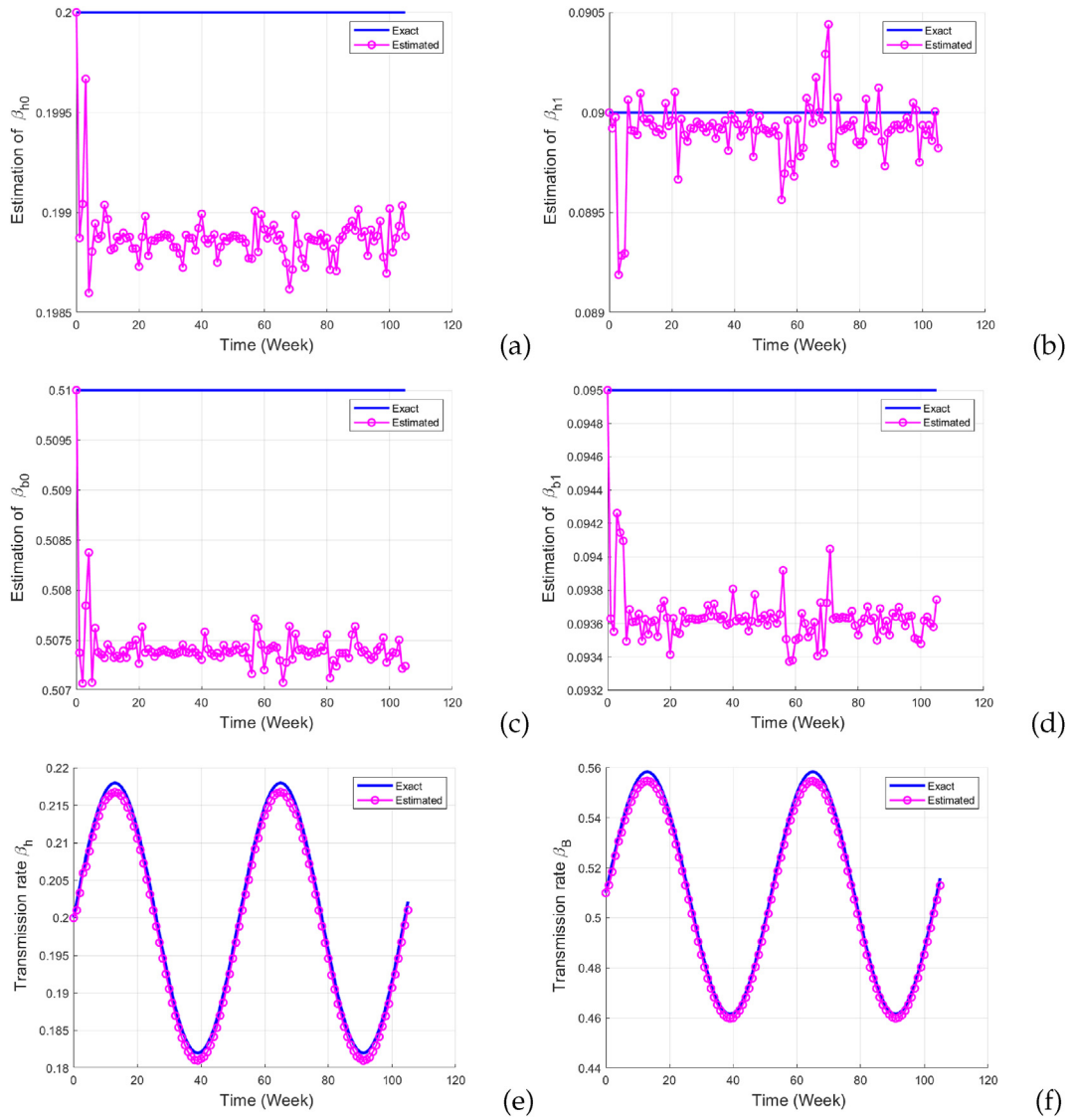

Fig. 3. Comparison between the exact value (blue line) and the estimated value (magenta line). (a)–(d) Semi-transmission rates β_{h0}, β_{h1}, β_{b0} and β_{b1}, respectively, (e) Transmission rate β_h and (f) Transmission rate β_b.

$S_0 = 23\,284\,799, I_{d0} = \mathcal{Y}_0 = 2, C_0 = 150, I_{u0} = 50, R_0 = 500$ and $B_0 = 100\,000$ so that $S_0 + I_{d0} + C_0 + I_{u0} + R_0$ corresponds to the total population of Cameroon in 2014 and where $\mathcal{Y}_0$ is the number of reported cases of cholera during the first week in 2014 in

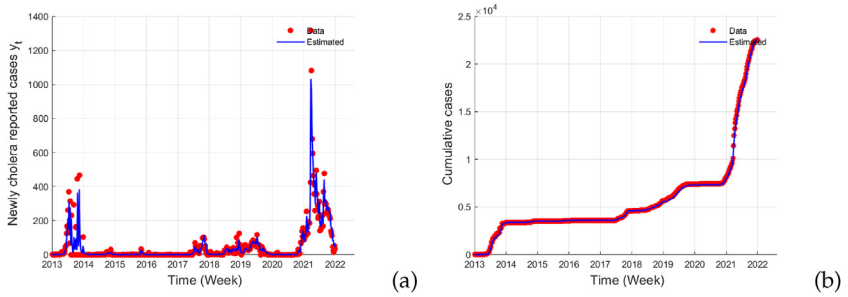

Fig. 4. Fitting real data of cholera from 2014 to 2022 in Cameroon using system (3). (a) Newly detected cases and (b) Cumulative cases.

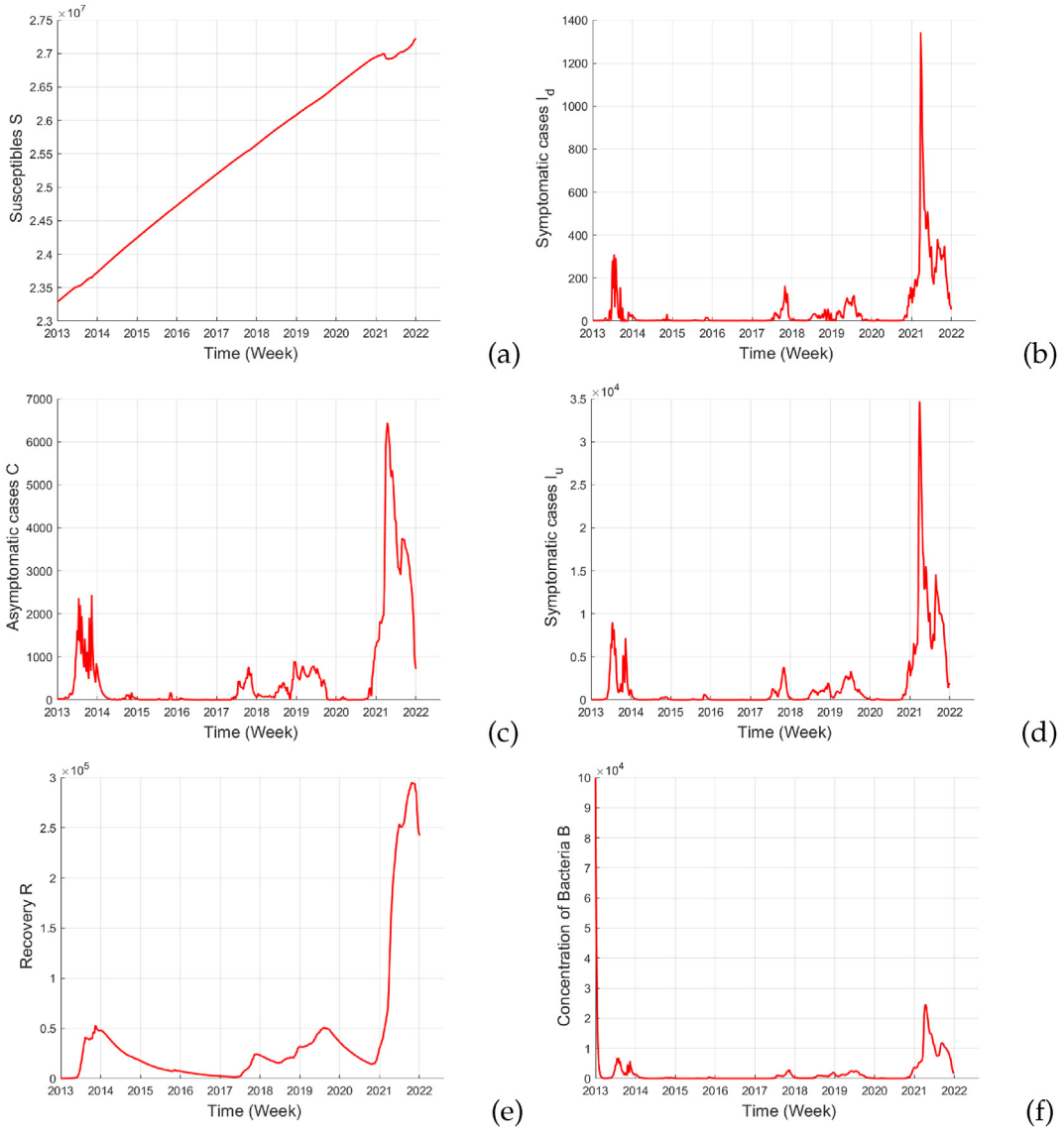

Fig. 5. Estimated states of cholera in Cameroon using system (20). (a) Susceptible individuals S, (b) Detected symptomatic cases I_d, (c) asymptomatic cases C, (d) Undetected symptomatic cases I_u, (e) Recovered individuals R and (f) Free *V. cholera* in the environment B.

Cameroon. Also, each estimation tool needs priori values of unknown parameters to begin the process. We choose the values that give the observation $\mathcal{Y}_0$ at the initial time with 10^{-5} as error, that is $\beta_{h0} = 0.078540$, $\beta_{h1} = 0.007547$, $\beta_{b0} = 0.000017$, $\beta_{b1} = 0.081811$, $\varepsilon_1 = 0.217941$, $\varepsilon_2 = 0.007845$, $\rho = 0.449524$, $\delta = 0.095029$, $\theta = 0.066538$, $\alpha = 0.143142$ and $\gamma_c = 0.053469$. Also, one assumes that: (i) the sample number to be $N = 100$ and (ii) the deviation matrices to be $Q_t = 25 \times I_6$, $R_t = 10^{-5} \times I_{10}$ and $Z_t = 2$ with I_n the identity matrix of size $n \in \mathbb{N}^*$.

Figs. 4–10 give the estimation results of cholera disease for both the state variables and unknown parameters in Cameroon. From Fig. 4, one sees that the estimated value (in blue line) fit well the available data (in red star). Thus, the estimation of periodic parameters and state variables of cholera in Cameroon using the *EnKf* design (20) is good. Firstly, one observes that susceptible individuals always increase in spite of cholera cases in Cameroon (see Fig. 5-(a)). Also, parameter values varie enough from their initial values (see Figs. 6–7) and the mean value is reported in Table 2 as estimation of unknown parameters. Fig. 8 present the reconstruction of other unknown parameters that could not estimated directly, but can be expressed from parameters in system (3). Fig. 8-(a) shows the human transmission rates (upper, average, instantaneous and lower values in blue, green, cyan and red lines, respectively) and, Fig. 8-(c) gives the comparison between transmission rates from symptomatic detected $\varepsilon_1\varepsilon_2\beta_h$, asymptomatic β_h and symptomatic undetected $\varepsilon\beta_h$ (see the blue, red and green lines, respectively). The reconstruction of the proportion ω of newly cholera cases with symptoms who are detected is depicted in Fig. 8-(d) and different transfers among asymptomatic cases in Fig. 8,(e) and (f)), respectively. Fig. 8 (a) and (b) show how the

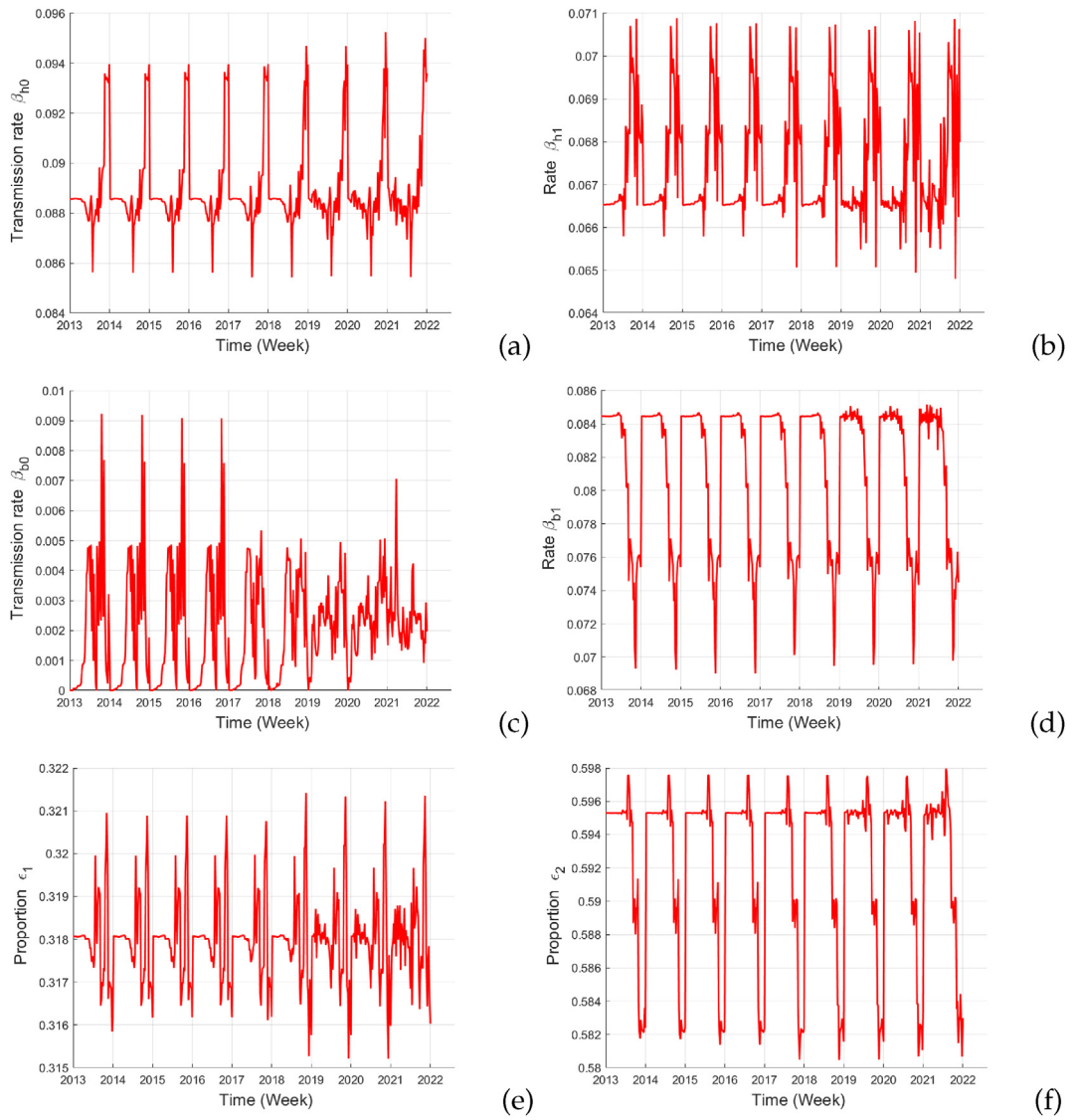

Fig. 6. Estimated parameters of cholera in Cameroon using system l (20). (a) mean transmission rate β_{h0}, (b) fluctuation amplitude β_{h1}, (c) mean transmission rate β_{b0}, (d) fluctuation amplitude β_{b1}, (e) proportion ε_1 and (f) proportion ε_2.

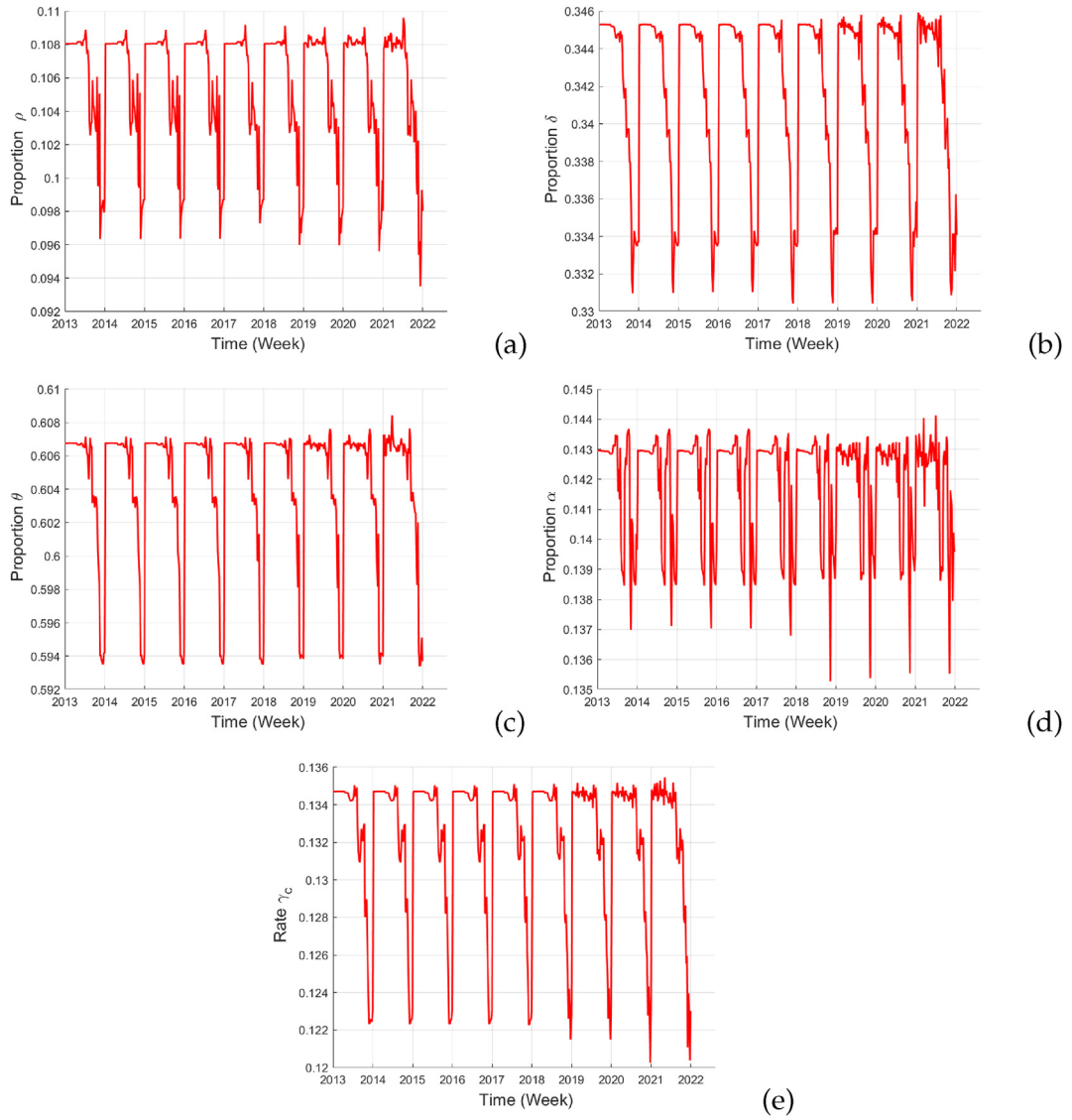

Fig. 7. Estimated parameters of cholera in Cameroon using system (20). (a) proportion ρ, (b) proportion δ, (c) proportion θ, (d) proportion α and (e) living rate of asymptomatic cases γ_c.

transmission rates $\beta_h(t) = \beta_{h0}\left(1 + \beta_{h1} sin\left(\frac{2\pi}{\tau_c} t\right)\right)$ and $\beta_b(t) = \beta_{b0}\left(1 + \beta_{b1} sin\left(\frac{2\pi}{\tau_c} t\right)\right)$ (in cyan lines) involve among theirs lowers and uppers bound (red and blue lines, respectively). We add the average values in green line ($\overline{\beta}_h = \beta_{h0}$ and $\overline{\beta}_b = \beta_{b0}$). Therefore, it can be seen that the majority of asymptomatic cases changes status without being registered by health personnel. However, the estimation of upper and lower value of effective reproduction number in Fig. 10-(a) shows the contribution of taking into account undetected symptomatic and asymptomatic cases not only on why we are always surprised to have more cases than expected when forecasting (look at the governmental forecasting plan if there are any). Indeed, a comparison of the different effective reproduction numbers (on average) affected by infectious human is given in Fig. 10-(c). Since that $\underline{\mathcal{R}}_0 \leq \mathcal{R}_0 \leq \overline{\mathcal{R}}_0$, it can be seen that $\mathcal{R}_{0c}$ and $\mathcal{R}_{0u}$ are 7 and 6 times greater than $\mathcal{R}_{0d}$, respectively ("this shows that infectious undetected are a great danger and that control should be taken"). Also, another comparative study shows that free *V. cholerae* in the environment are responsible of more cholera spread than infectious individuals; maybe because humans are largely responsible for bacterial deposits in the environment (see the blue and ref lines in Fig. 10-(b)). The mean values of estimated parameters are reported in Table 2 (see Fig. 12).In Fig. 9, we give a comparison of cholera cases in Cameroon from 2014 to 2022. It shows that active asymptomatic cases reach their maximum values at the end of each outbreak period (see the peak in green line in Fig. 9-(b)). These values are two times greater than peak of symptomatic undetected and eight times the detected cases, approximately. In additional, Fig. 9-(b) shows that in absence of outbreak,

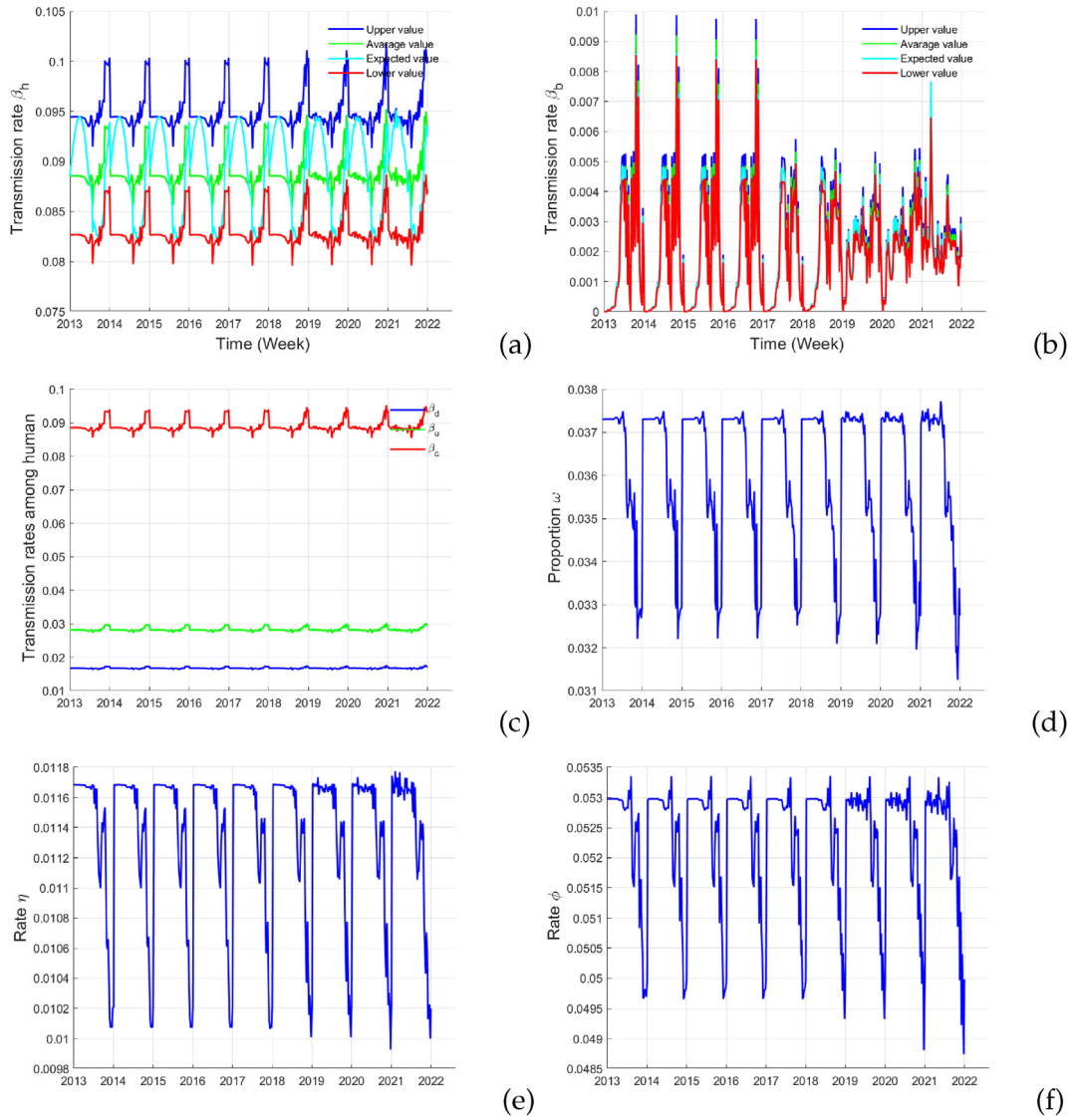

Fig. 8. Reconstruction of transmission rates from cholera in Cameroon. (a) transmission rate β_h, (b) transmission rate β_b, (c) Comparison of transmission rates from human, (d) proportion of newly detected symptomatic cases $\omega = \rho\delta$, (e) detection rate of asymptomatic cases $\eta_c = \theta\alpha\gamma_c$ and (f) recovery rate of asymptomatic cases $\varphi_c = \theta(1-\alpha)\gamma_c$.

there are sufficient asymptomatic cases of cholera. However, cumulative cases from undetected symptomatic are more important than that from detected and it is same with cumulative deceased cases (see blue and red lines in Fig. 9-(c) and (d)).

Since that the mean value of sous-estimating effective reproduction number is largely greater than 1 ($\underline{\mathcal{R}}_0 = 1.6527$), it is important to predict the evolution of cholera in Cameroon.

3.4. Forecasts of cholera in Cameroon

In the previous step, the results planed the continuation of the pandemic since that the effective reproduction number is greater than the unity. In this step, we aim to present the forecasts of the cholera disease in Cameroon. To do this, we use the estimated parameters and state variables obtained in the previous section. The states at the end of estimation (see Table 3) are considered as the initial condition in system (3) for the forecasts of cholera disease in Cameroon from January 2023 to December 2024. Also, we use the values of parameters reported on Table 1 and the mean values of unknown parameters reported in Table 2.

The trends show that cholera pandemic will decrease at the end of 2023 but, will reappear in 2024 (see red and blue line in Fig. 11-(a)–(f)). However, it is possible that the pandemic disappears, since that the threshold $\underline{\mathcal{R}}_0$ can be less than the unity at

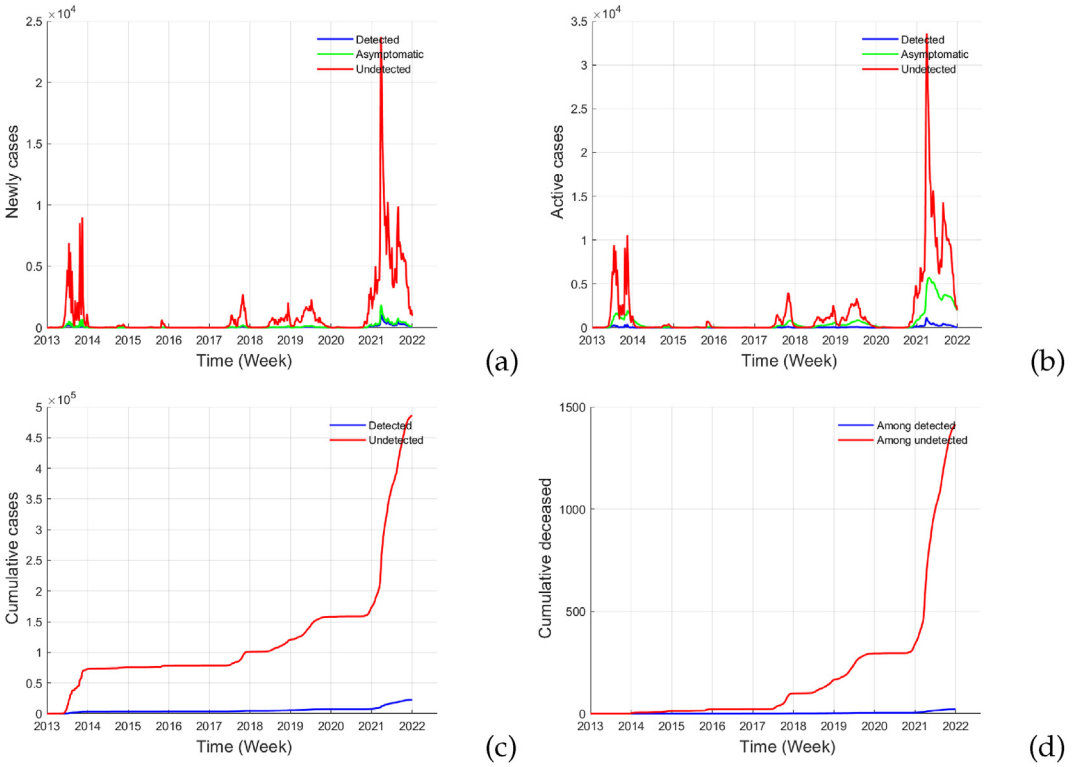

Fig. 9. Reconstruction and comparison of cholera cases in Cameroon. (a) Newly cases, (b) Active cases, (c) Cumulative cases and (d) Cumulative deceased.

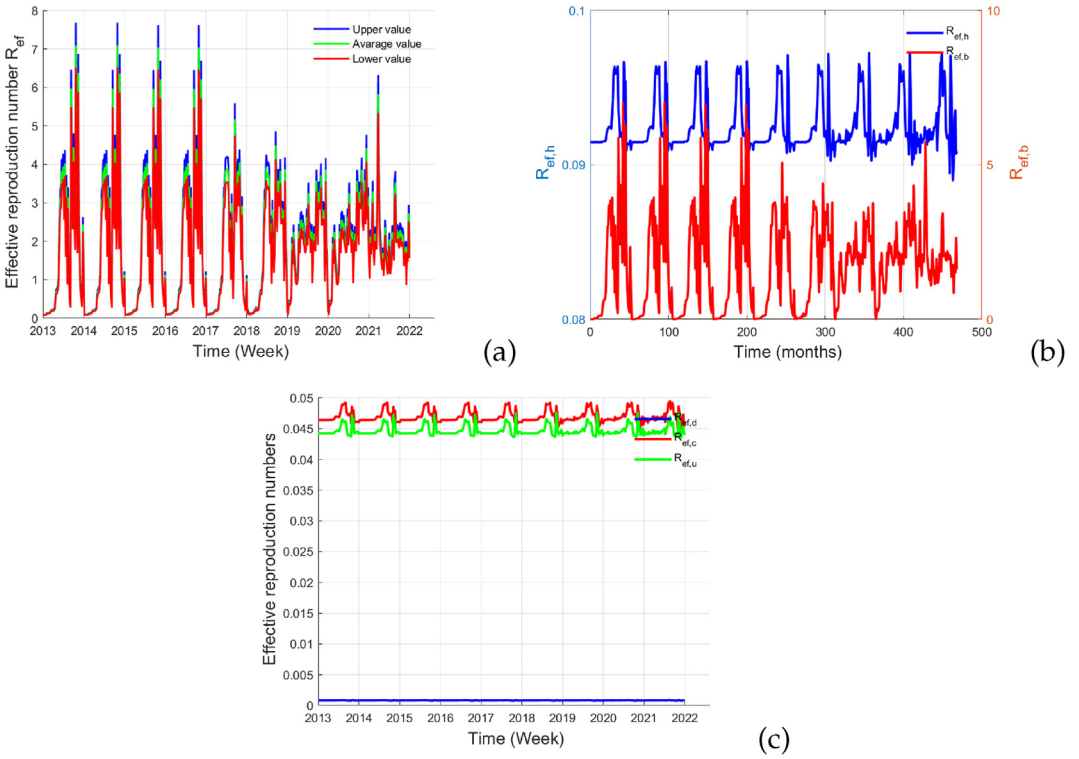

Fig. 10. Estimation of the effective reproduction numbers of cholera from 2014 to 2022 in Cameroon. (a) Upper, average and lower value of effective reproduction number $\mathcal{R}_{ef}$, (b) Comparison between average value $\mathcal{R}_{ef,h}$ and $\mathcal{R}_{ef,b}$ and (c) Comparison between average values of $\mathcal{R}_{ef,d}$, $\mathcal{R}_{ef,c}$ and $\mathcal{R}_{ef,u}$.

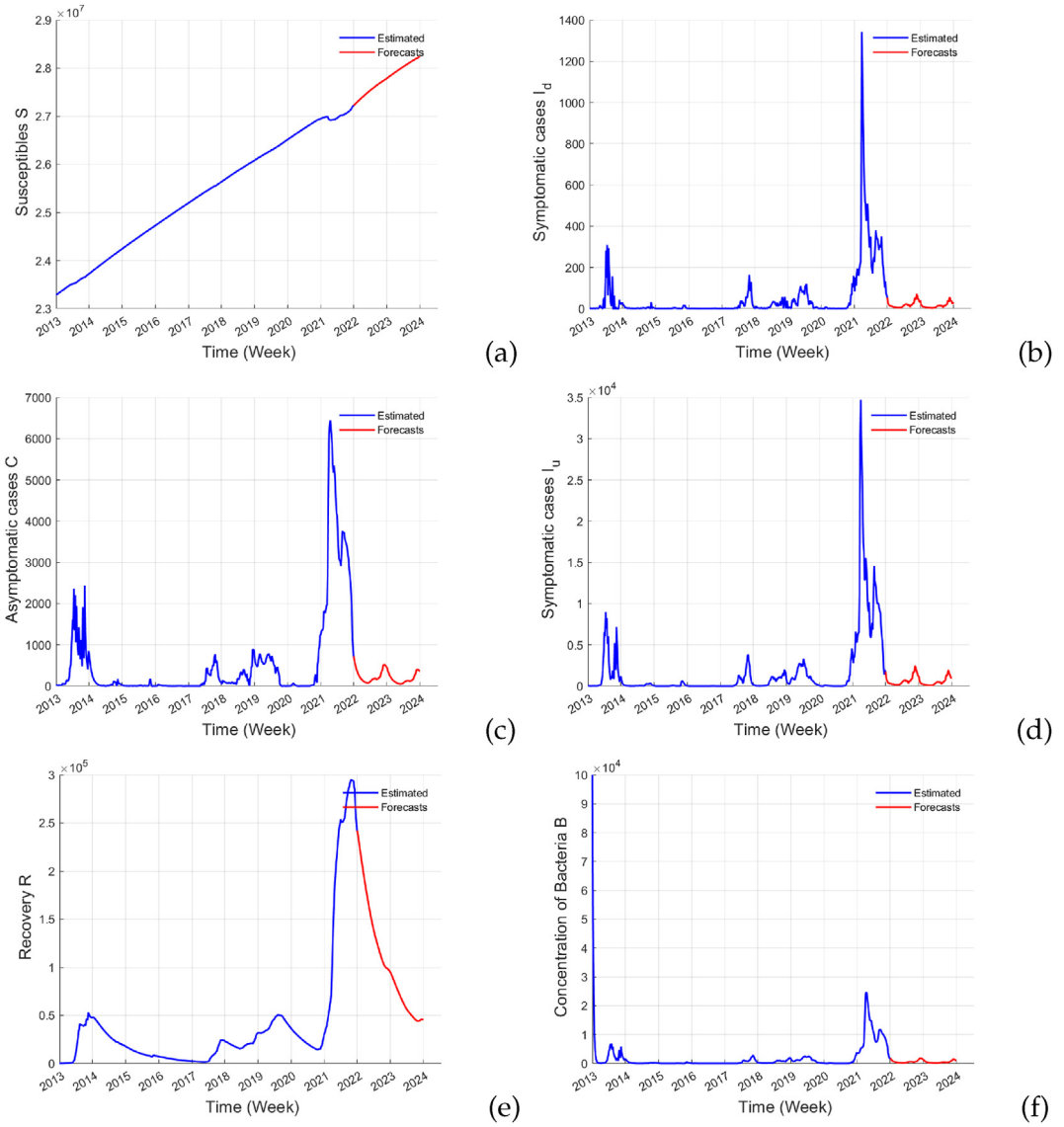

Fig. 11. Forecasts of cholera system (3) in Cameroon from January 2023 until December 2024. (a) Susceptible individuals S, (b) Detected symptomatic cases I_d, (c) Asymptomatic cases C, (d) Undetected symptomatic I_u, (e) Recovered individuals R and (f) Free *V. cholerae* in the environment B.

Table 2
Mean values of estimated parameters of cholera in Cameroon from 2014 to 2022.

Parameters	Values	Parameters	Values	Parameters	Values
β_{h0}	0.08989	ρ	0.10294	η	0.01153
β_{h1}	0.06499	δ	0.34321	φ	0.05360
β_{b0}	0.00210	θ	0.60359	$\overline{\beta}_h$	0.09573
β_{b1}	0.08374	α	0.14133	$\underline{\beta}_h$	0.08405
ε_1	0.31554	γ_c	0.13520	$\overline{\beta}_b$	0.00205
ε_2	0.59251	ω	0.03536	$\underline{\beta}_b$	0.00193
$\underline{\mathcal{R}}_{0d}$	0.00077	$\overline{\mathcal{R}}_{0d}$	0.00088	$\underline{\mathcal{R}}_{0c}$	0.04401
$\overline{\mathcal{R}}_{0c}$	0.05013	$\underline{\mathcal{R}}_{0u}$	0.04165	$\overline{\mathcal{R}}_{0u}$	0.04744
$\underline{\mathcal{R}}_{0h}$	0.08644	$\overline{\mathcal{R}}_{0h}$	0.09845	$\underline{\mathcal{R}}_{0b}$	1.65628
$\overline{\mathcal{R}}_{0b}$	1.85044	$\underline{\mathcal{R}}_0$	1.65272	$\overline{\mathcal{R}}_0$	1.94890

some period (see his evolution on Fig. 10-(a)). Also, it illustrates that the incidence could be very small if a control strategy is applied so that that unknown parameters reach the mean values of their estimates. Indeed, we use the mean values of

Table 3
Estimated states of system (3) for the last week of 2022.

variables	S	I_d	C	I_u	R	B
Values	27 225 889	53	718	1743	242 095	1758

Table 4
States of cholera in Cameroon on December 2022.

Variables	Detected symptomatic cases		Asymptomatic		Undetected symptomatic cases	
States	New	Active	New	Active	New	Active
Values	2 343 180	β_{h0}	0.02799	β_H	0.02702	

Table 5
Performance of prevision of cholera in Cameroon.

Names	Estimation	Prediction
MAE	9.32210	9.65268
RMSE	23.74199	12.85877
Nash Ef. Er.	0.75099	0.45964

Table 6
Numerical values used for the impulsive controls in Eq. (22).

p	β_{h0}	β_{b0}	$1-\mu_b$	ξ_d, ξ_c, ξ_u
r_p	0.03	0.03	0.03	0.03
$\overline{p}$	0.08989	0.08374	4/10	0.75
p_0	0.098	0.168	2/10	0.5

unknown parameter for the forecasts. The estimations and forecasts show that deceased are more important among undetected cases than detected cases (see the red and blue lines in Fig. 12-(c)). In this work, we take into account asymptomatic and undetected symptomatic cases of cholera in the context of sub-Saharan Africa and we use data from Cameroon for the application. Thus, it is difficult to compare the results obtained and the *EnKf* method to calibrate the cholera model and we do not have any results in this way available in the literature for a comparison. To appreciate the estimation and forecasts processes in Cameroon with the *EnKf* in system (20), one evaluates the following errors for $N \in \mathbb{N}^*$ observed data (Y_{Ob}) and its estimates (Y_{Est}):

a. Mean Absolute Error *MAE*: $(1/N)\sum_{i=1}^{N} |Y_{Ob}(i) - Y_{Est}(i)|$.

b. Root Mean Square Error *RMSE*: $\sqrt{(1/N)\sum_{i=1}^{N} (Y_{Ob}(i) - Y_{Est}(i))^2}$.

c. Nash Efficient Error *Nash Ef. Er.*: $1 - \sum_{i=1}^{N} (Y_{Ob}(i) - Y_{Est}(i))^2 / \sum_{i=1}^{N} (Y_{Est}(i) - \overline{Y}_{Ob})^2$.

The results are reported on Table 5. It is clear that one has a good appreciation and the Nash efficient error give that the estimation of observed data is done for more than 75% of data and give at 45% for forecasts.

Since that the forecasts showed the possibility to observe cholera cases each year, it will be important to apply control strategies that can help to avoid its.

3.5. Control strategies

Here, we consider the problem of control of cholera disease by reducing transmission rates either from infected individuals or from free *V. cholerae* in the environment through applying barrier measure. In addition, reduce or eradicate the pathogens in player area or surface, public places and chlorinate soil foot or water. The aim is to reduce the number of infectious cases as follows.

Two methods of control are applied: education and sanitation. Education consists to reduce the contacts of susceptible individuals with *V. cholerae*. So, the parameters affected for this control are the transmission rates β_h and β_b. In other side, sanitation is applied to eradicate the bacterial in surfaces, food and water. In fact, the effect is done to increase the mortality μ_b in system (3). Therefore, control actions consist to increase the values μ_b and to decrease the values of β_{h0} and β_{b0} when risk factors of cholera outbreaks appear during outbreak. The control of β_{h0} and β_{b0} affect the involve of transmission rates β_h and

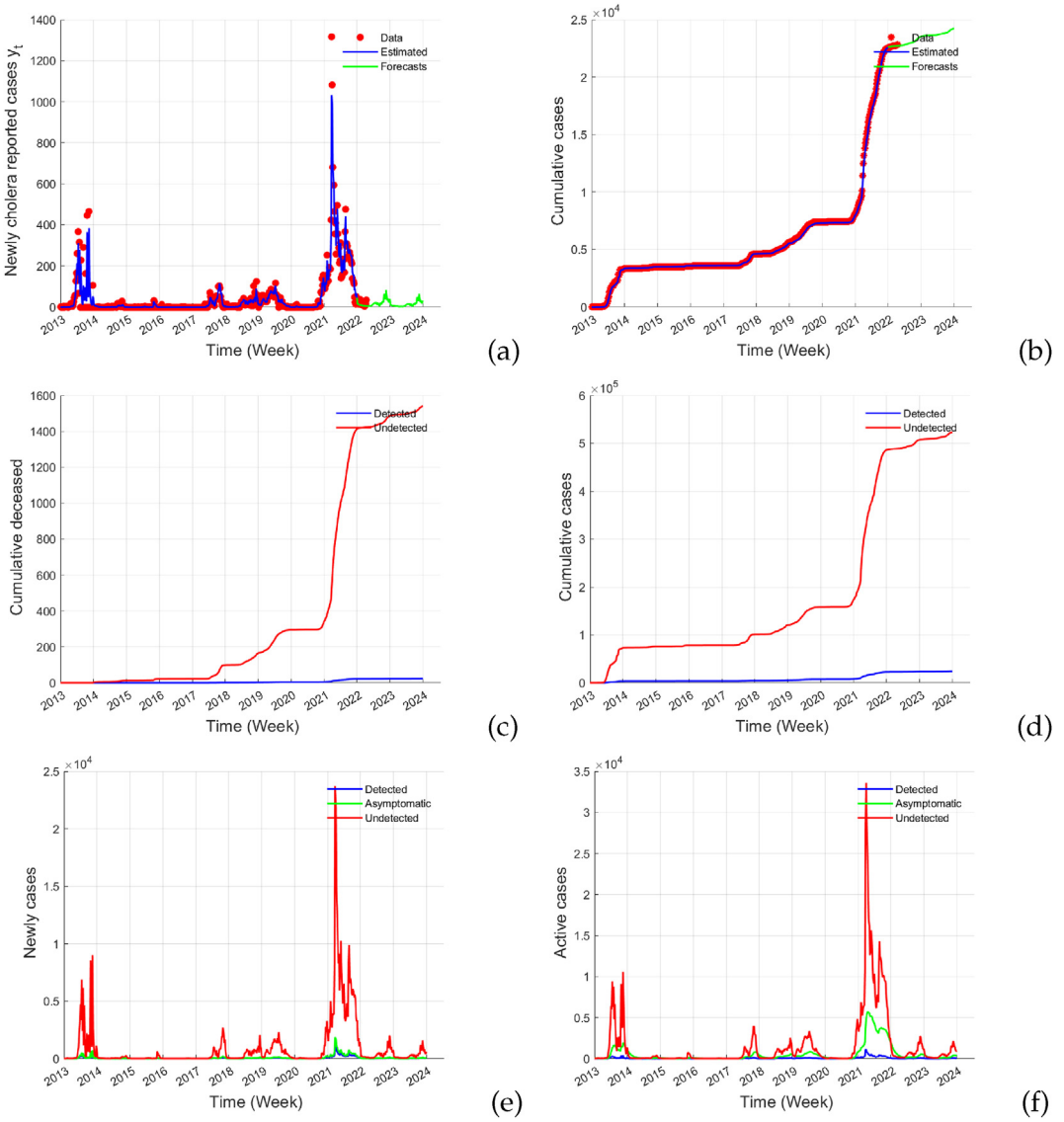

Fig. 12. Forecasts of cholera cases in Cameroon from January 2023 until December 2024. (a) Newly detected cases and (b) Cumulative detected cases, (c) Cumulative deceased cases, (d) Cumulative cases, (e) Newly cases and (f) Active cases.

β_b, respectively. At the end, the control is directly linked to the parameters, but not throughout the epidemic period, but rather at regular intervals. These are the impulses for each parameter to be monitored. This type of control has already been applied by Dumont et al. and Kolaye et al. (Dumont & Thuilliez, 2016; Kolaye, Damakoa, Bowong, Houe, & Békollè, 2020). We use the same principle to decrease the parameter $p \in 1 - \mu_b, \beta_{h0}, \beta_{b0}$ by considering the mean parameter $\overline{p}$ and the growth rate r_p of p. p is the solution of the following equation:

$$\begin{cases} \dot{p} = r_p(\overline{p} - p), \\ p(t_0) = p_0. \end{cases} \tag{21}$$

Assuming that a proportion Θ of human population agrees to apply control strategies, one supposes that these actions are applied dependently of time. So, the result in (Kolaye et al., 2020) gives that the impulsive control $p(t)$ is a periodic function and is

$$p(t) = \begin{cases} \overline{p} - (\overline{p} - p_0)\exp(-r_p t), & \text{if } t \in [0, t_0] \\ \overline{p} - (\overline{p} - (1 - \psi(\Theta))p((n-1)T + t_0))\exp(-r_p(t - (n-1)T - t_0)), & \text{if} \\ & t \in](n-1)T + t_0, nT + t_0], \quad n = 1, 2, \ldots \end{cases} \tag{22}$$

where t_0 represents the time on which start the control and ψ is chosen as follows:

$$\psi(\Theta) = \frac{a\Theta}{1 + a\Theta}, \qquad \text{with } a > 0.$$

Remark 2. ψ could be any non-decreasing function among $[0, 1]$ with $\psi(0) = 0$ and $0 < \psi(1) < 1$.

The model with controls is obtained by replacing β_{h0}, β_{b0} and μ_b by time-varying $\beta^*_{h0}(t)$, $\beta^*_{b0}(t)$ and $\mu^*_b(t)$, respectively in system (3).

The application is done by taking β_{h0} and β_{b0} as the last value obtained at the end of estimation (in fact, we start the control process on first January 2023). The results are given for the forecasts joining control action and without control with value of r_p, $\overline{p}$ and reported on Table 6.

From Fig. 13, it is evident that, the control has a good impact both in the free Free *V. cholerae* and incidence of cholera in Cameroon. In fact, the control of ξ_d, ξ_c and ξ_u are decreasing for the two year of prevision (see the red and blue line in Fig. 13-(a)). Also, the comparison studies in Fig. 13 (b)–(d) shows that a periodic control on contact rates reduce the incidence of cholera and this significantly. The same result can be seen in Fig. 13-(e)) where the deceased cases without control are two

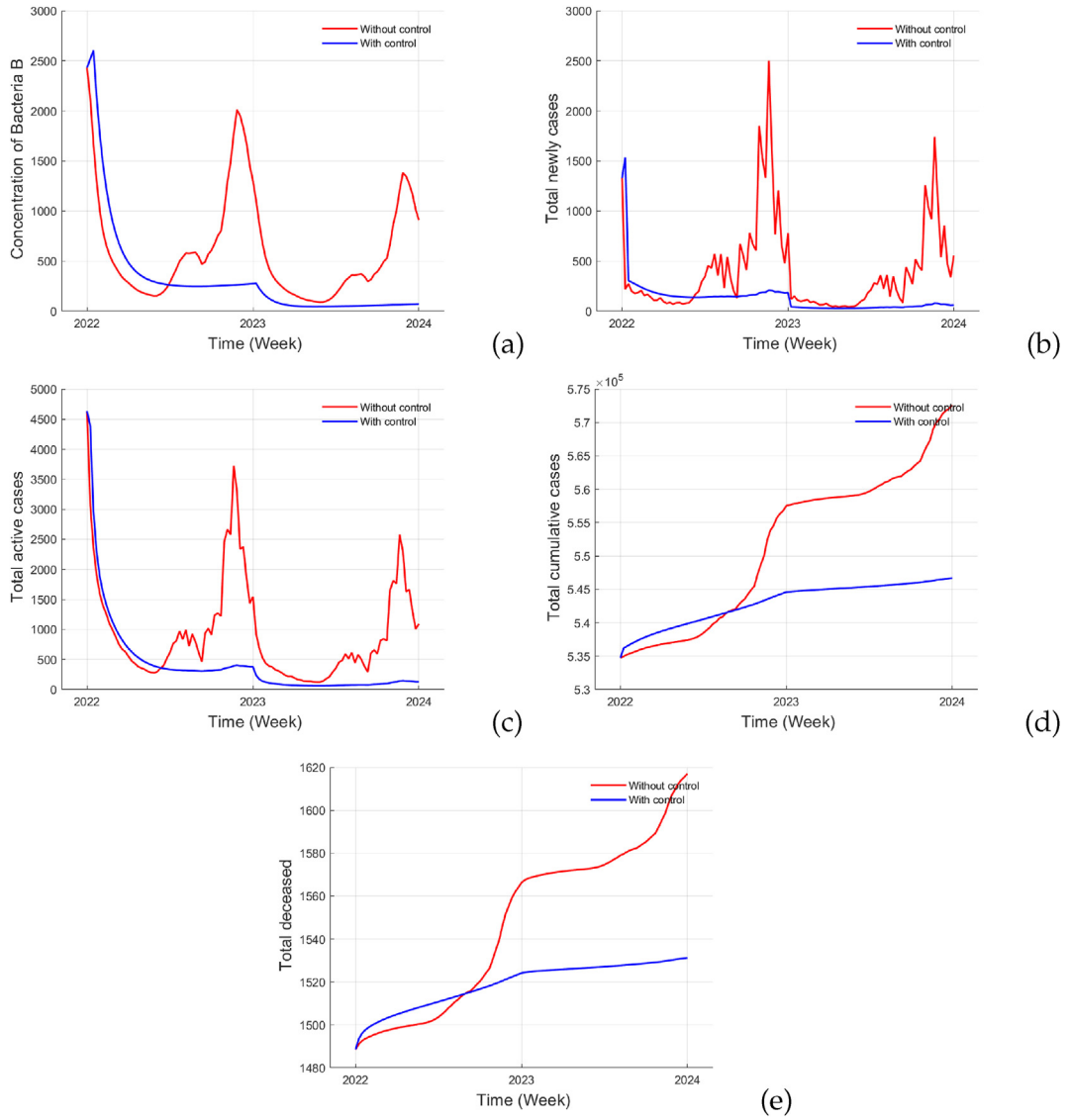

Fig. 13. Trajectories of cholera disease in Cameroon from January 2023 to December 2024 when there is no intervention and when control strategies are applied. (a) Free *V. cholerae* in the environment, (b) total newly cases, (c) total active cases, (d) total cumulative cases and (e) total deceased cases.

times greater than when control are applied. In addition, one can observe. that there will not be waves or another increasing outbreak with the impulsive controls taken.

4. Conclusion

This paper has addressed the problem of the prediction and control of cholera outbreak. We first proposed a mathematical model of cholera than can be adapted in most countries of sub-Saharan Africa. The model incorporated the following factors: (i) undetected symptomatic cases who developed cholera symptoms directly after the inoculation of *V. cholerae* but, aren't detected for several reason; (ii) asymptomatic cases are supposed to be unknown far into the apparition of symptoms if they aren't recovered and (iii) seasonal transmission from either infected individuals or free *V. cholerae* in the environment. A qualitative analysis of the model has been presented such as the integral operator which gives the effective reproduction number, the existences and stabilities of the disease free equilibrium. Also, one gave a less-estimation and upper-estimation of the effective reproduction number. After, one models the estimation problem using the available data of cholera which are the newly reported cases. And, we use the approach of *EnKf* for dual estimation when parameter is supposed to vary periodically per year. We apply the method to the real data of cholera cases in Cameroon to estimate the total cases and parameters which rested unknown in Cameroon. In additional, we use the estimated variables to reconstruct the active and the deceased among undetected cases in Cameroon from 2014 to 2022. At the end, estimated parameters and state variables at the end of 2022 have been used in the dynamic of cholera to forecasts the trajectories of the diseases in Cameroon until 2024 in when prevention strategies in term of impulsive controls are applied or not. Results could be founded as following.

1 We have computed the disease-free periodic solution and derived the basic reproduction number $\mathcal{R}_9$ using the theory of (Bacaër & Guernaoui, 2006). Because that basic reproduction number formula was not explicit, we have proved that it can be bounded by two explicitly computed threshold parameters $\underline{\mathcal{R}_0}$ and $\overline{\mathcal{R}_0}$ such that $underline\mathcal{R}_0 \leq \mathcal{R}_0 \leq \overline{\mathcal{R}_0}$. We have shown that the disease-free periodic solution is locally asymptotically stable whenever $\mathcal{R}0 < 1$, and unstable if $\mathcal{R}_0 > 1$. We have established that, as long as $\overline{\mathcal{R}_0} < 1$, the disease tends to disappear from the population and otherwise $(\overline{\mathcal{R}_0} > 1)$, the disease persists uniformly in the population.
2 We reconstructed the new infected cases although having their values, in order to appreciate the estimates made on the state variables and parameters of each model. The estimated function of newly reported cases follows those of real data (see green line and red stars in Fig. 11-(a) and (b)); this result gives a good appreciation of estimated values of the unmeasurable variables and unknown parameters in system (3). From these graphs, one can see that the absence of cholera cases from 2015 to the middle of 2018 is due to: the fact that the concentration of free *V. cholerae* in the environment was insufficient to trigger the outbreak during these period (see Fig. 5-(b)) and to a few number of asymptomatic. This is due to the fact that the epidemic caused tremendous fear among the population who subsequently took control through the application of goodness hygiene of life. On the other hand, the absence of water channels in the city of Cameroon and the presence of garbage everywhere have favoured the multiplication of the *V. cholerae* in the environment over time that triggered new outbreak on 2018. The large mass of the population in Cameroon contributed to the dissemination of the cholera epidemic and the increasing of *V. cholerae* in the environment. The results obtained show how transmission from bacteria is more important than that from human (see Fig. 10-(b)). Thus, indirect contacts should be limited (as in the case of COVID-19) in an epidemic situation, even though the outbreak is triggered through symptomatic undetected and more trough Asymptomatic cases. Also, cholera outbreak affects the increasing of susceptible individuals incidence (see the evolution on during 2021 and 2022 in Fig. 5-(a)). The confirmation of the above analyses can be observed on the evolution in average of the effective reproduction number through human $\mathcal{R}_{0h}$ and the one through free *V. cholerae* in the environment (see Fig. 10-(b)). Also, one observes the almost periodicity with decreasing amplitude of the values of estimated $\mathcal{R}_0$ which involves around two but, stays for long time less than the unity each year. This shows that even in absence of epidemic within human population, the *V. cholerae* continuous to be sheeted in environment. This analyze is appreciated by looking of Isaac Chun-Hai Fung (Isaac, 2014) who founded that there are some asymptomatic individuals who continuous to shed *V. cholerae* in the environment even in absence outbreak. The state values of cholera in the city of Cameroon on December 2022 are reported in Tables 3 and 4 We observed that either in absence or with cholera disease, human transmission rate β_h increased on December (see Fig. 8-(a)). Thus, each year the risk of infection within human population is on December maybe due to that it is the period of festivities. Also, we found that asymptomatic cases transmit five and three times more than symptomatic detected and undetected, respectively. However, the transmission from free *V. cholerae* begin to be high few week after May and in October (see the peak in Fig. 8-(b)). indeed, at this time of each year, there are some rainfalls in Cameroon, which carry *V. cholerae* from their homes to the populations since as there is no canalisation available. Thus, a good control strategy would be to apply monitoring and awareness process at this time. Also, one estimates that 90% of newly infected cases have symptoms but aren't diagnosed since that the are many diarrhoeic disease in sub-Saharan regions in Africa. Elsewhere, 60.36% of asymptomatic are detected after (14%) or recover naturally (86%). Even if the incidence is small, it is important to continue awareness against cholera since that the forecasts give that after the current 2023 outbreak, it is possible to observe such waves (due to that the lower value of effective reproduction number $\underline{\mathcal{R}_0} \approx 1.67144$). Besides, the model has the capacity to predict each incidence of cholera epidemic, that depends on the states and parameters estimated.

3 Finally, we have incorporated two control actions into our model, namely (i) awareness of people to avoid contacts of people with *V. cholerae* and (ii) pouring the chlorine in areas infected by the *V. cholerae* such as water wells, traditional latrines, etc. The simulation of the model with the control strategy from January 2023 to December 2024 show (a) a reduction of more than 75% of the incidences and the disappearance of the peaks when no control are available In the first year of monitoring; and (b) a reduction of around 60% t of the incidences when a second monitoring of control is applied. In addition, we note that these absences and periodic application of sanitation in water will cause free bacteria to disappear from the environment. In this way, we will be able to substantially reduce this pandemic (which dates back to the 1970s) from Cameroon. However, all this results can be improve with available data of weekly recovered and deceased of cholera cases in Cameroon.

CRediT authorship contribution statement

C. Hameni Nkwayep: Writing – review & editing, Writing – original draft, Data curation, Conceptualization. **R. Glèlè Kakaï:** Writing – review & editing, Supervision, Methodology. **S. Bowong:** Writing – review & editing, Supervision, Methodology.

Declaration of competing interest

We wish to submit an original research article entitled "Prediction and control of Cholera outbreak: study case of Cameroon" for consideration by *Infectious Disease Modelling* journal.

We confirm that this work is original and has not been published elsewhere, nor is it currently under consideration for publication elsewhere.

In this article, we report that asymptomatic and undetected symptomatic cases of Cholera and free *Vibrio cholerae in the environment* are important variables in the controlling process of Cholera diseases in Sub-Saharan Africa: Cameroon for example. Also, that periodical estimation on parameters could improve the prevision of Cholera. This is important because it is necessary to take into account climatic factor as seasonal rates to increase awareness of individuals about new outbreak and currently detect new infectious of Cholera that will decrease the total prevalence (detected and undetected) in the future.

We believe that this manuscript is appropriate for publication by *Infectious Disease Modelling* because it contribute to three main axes of yours thematic: epidemiology, infectious diseases and estimation.

Cholera is considered as a pandemic in some countries of Sub-Saharan Africa and its different apparitions sufficiently show that it would be necessary to estimate several parameters that could help to evaluate the number of undetected cases of Cholera with an epidemiological model. Also, this would allow us to better estimate the basic reproduction number and thus better give forecast.

In this work, we propose and analyze a compartmental model of Cholera to predict and control the outbreak in the context of sub-Saharan Africa. We use really data of number of newly detected cases of Cholera in an Ensemble Kalman filter design to estimate at time unmeasured variables and unknown parameters in Cameroon. Also, we present the forecasts of the current pandemic in Cameroon without and with impulse controls. The results suggest that the disease would better decrease in Cameroon with control measures in term of sanitation and hygiene practices.

We have no conflicts of interest to disclose.

Acknowledgements

Hameni Nkwayep Cedric acknowledges the support of the African-German Network of Excellence in Science (AGNES) for granting a Mobility Grant in 2022; the Grant is generously sponsored by German Federal Ministry of Education and Research and supported by the Alexander von Humboldt Foundation.

Appendix A. Proof of theorem 1

In this part, we study the basic properties of system which is essential in the proofs of stability results. So, we prove in this part that any solution of system (3) with a positive initial condition remains non negative and bounded.

The proof of theorem 1 is done in three steps as that follows.

Step 1: We show that the solution $X(t)$ of system (3) corresponding to initial conditions such that $X(0) > 0$ are non negative for all $t > 0$.

Suppose that $X(0) > 0$. Then from the model equation and properties of continuous functions, there exists some $t_0 > 0$ so that $X(t)$ remain non-negative for all $t \in [0, t_0]$. We are now going to show that $t_0 = \infty$.

Suppose that $t_0 < \infty$. Hence, there exists $t_1 \geq t_0$ which vanish at least one component of X. We define

$$t^* = \inf\{t_1 \geq t_0 : S(t_1) = 0, \text{ or } I_d(t_1) = 0, \text{ or } C(t_1) = 0, \text{ or } I_u(t_1) = 0, \text{ or } R(t_1) = 0, \text{ or } B(t_1) = 0\}.$$

Suppose that $S(t^*) = 0$ and let us consider the first equation of system (3):

$$\dot{S}(t) = \Lambda + \sigma R(t) - (\lambda(t) + \mu)S(t), \qquad \forall t \in [0, t^*].$$

Using the definition of t^* and the above equation, one has that

$$\dot{S}(t) + (\lambda(t) + \mu)S(t) > 0.$$

Integrating the above inequality from 0 to t^*, one can deduce that

$$\int_0^{t^*} \frac{d}{dt}\left[S(t)\exp\left(\int_0^t \lambda(s)ds + \mu t\right)\right] > 0.$$

Since $S(0) > 0$, one has that

$$S(t^*) > S(0)\exp\left(-\int_0^{t^*} \lambda(s)ds - \mu t^*\right) > 0,$$

which is a contradiction with the fact that $S(t^*) = 0$. Using the same arguments, we prove by the absurdity of $t_0 < \infty$ that $I_d(t^*) > 0, C(t^*) > 0, I_u(t^*) > 0, R(t^*) > 0$ and $B(t^*) > 0$. This implies that $X(t)$ remain non-negative for all $t \in [0, t_0[$. Therefore, the trajectories of the solutions of system (3) remain positive for all $t \in [0, e + \infty[$.

Step 2: We prove that the total population of humans and the concentration of Bacteria in the environment at time t, $N(t)$ and $B(t)$ respectively are bounded.

1 Adding the first, second and the third equations in system (3), the dynamic of total human population satisfies

$$\dot{N}(t) = \Lambda - \mu N(t) - d_d I_d(t) - d_u I_u(t) \leq \Lambda - \mu N(t). \tag{23}$$

Applying the Gronwall inequality to the above differential inequality (23) with the initial condition $N(0)$, it yields

$$N(t) \leq \frac{\Lambda}{\mu} + \left(N(0) - \frac{\Lambda}{\mu}\right)e^{-\mu t}, \quad \forall t \geq 0. \tag{24}$$

implies that $N(t) \leq \frac{\Lambda}{\mu}$ for all time $t \geq 0$ if $N(0) \leq \frac{\Lambda}{\mu}$.

2 Finally, using the last equation of system (3) and the fact that $I_d(t), C(t), I_u(t) \leq \frac{\Lambda}{\mu}$, for all time $t \geq 0$, one has that

$$\dot{B}(t) \leq \frac{\Lambda}{\mu}(\xi_d + \xi_c + \xi_u) - \mu_B B. \tag{25}$$

Applying again the Gronwall inequality to (25) as in Eq. (23), it comes that $B(t) \leq \frac{\Lambda}{\mu\mu_B}(\xi_d + \xi_c + \xi_u)$ for all $t \geq 0$ if the initial condition $B(0)$ is less than $\frac{\Lambda}{\mu\mu_B}(\xi_d + \xi_c + \xi_u)$.

Therefore, combining *Step 1* and *Step 2*, the result about the positivity and the boundedness of solutions resumed in (4) is proved.

Step 3: Here, one shows how the system (3) admits a unique maximal solution. Firstly, it exists a constant $n_0 > 0$ such that the dynamic of total population verifies $N(t) \geq n_0$.Suppose that $\forall n_0 > 0$, it exists $t_0 > 0$ such that $N(t_0) < n_0$.

Using the dynamic of N in (23) and the fact that $I_d(t), I_u(t) \leq N(t)$, $\forall t \geq 0$, it follows that

$$\dot{N}(t) \geq \Lambda - (\mu + d_d + d_u)N(t). \tag{26}$$

The Gronwall inequality to the above differential inequality (26) with the initial condition $N(0)$ gives that

$$N(t) \geq \frac{\Lambda}{\mu + d_d + d_u} + \left(N(0) - \frac{\Lambda}{\mu + d_d + d_u}\right)e^{-(\mu+d_d+d_u)t}, \quad \forall\, t \geq 0.$$

At $t = t_0$, one has:

$$N(t_0) \geq n_0,$$

where

$$n_0 = \frac{\Lambda}{\mu + d_d + d_u}\left(1 - e^{-(\mu+d_d+d_u)t_0}\right) + N(0)e^{-(\mu+d_d+d_u)t_0}.$$

Which is absurd since that one supposes that $N(t_0) < n_0$, for all $n_0 > 0$.

So, $N(t)$ is asymptotically different to zeros. This implies that the right part of system (3) is $C^\infty(\Omega)$, thus locally Lipschitzian. This complete the proof of Theorem 1.□

Appendix B. Basic reproduction number of system (3)

Here, we present a theory of time varying system and compute a monodromy matrix used to give the integral operator of the basic reproduction number.

Basic reproduction number properties for periodic system

Here, we present the theory of the basic reproduction ratio for periodic compartmental models. For this all the following purpose must be verify (Diekmann et al., 1990).

We consider a heterogeneous population whose individuals can be grouped into n homogeneous compartments. Let $x = (x_1, \ldots, x_n)^T$, with each $x_i \leq 0$, be the state of individuals in each compartment. We assume that the compartments can be divided into two infected types, labelled by $i = 1, \ldots, m$, and uninfected compartments, labelled by $i = m + 1, \ldots, n$. Define X_s to be the set of all disease-free states:

$$X_s := \{x \geq 0 : x_i = 0, \forall\, i = 1, \ldots, m\}.$$

Let $\mathcal{F}_i(t,x)$ be the input rate of newly infected individuals in the ith compartment, $\mathcal{V}_i^+(t,x)$ be the input rate of individuals by other means (for example, births, immigrations), and $\mathcal{V}_i^-(t,x)$ be the rate of transfer of individuals out of compartment i (for example, deaths, recovery and emigrations). Thus, the disease transmission model is governed by a non autonomous ordinary differential system:

$$\frac{dx_i}{dt} = \mathcal{F}_i(t,x) - \mathcal{V}_i(t,x) = f_i(t,x), \qquad i = 1, \ldots, n, \tag{27}$$

where $\mathcal{V}_i(t,x) = \mathcal{V}_i^+(t,x) + \mathcal{V}_i^-(t,x)$. We make the following assumptions:

(A1) For each $1 \leq i \leq n$, the functions $\mathcal{F}_i(t,x)$, $\mathcal{V}_i^+(t,x)$ and $\mathcal{V}_i^-(t,x)$ are non negative and continuous on $\mathbb{R} \times \mathbb{R}_+^n$ and continuously differential with respect to x.
(A2) There is a real number $\omega \geq 0$ such that for each $1 \leq i \leq n$, the functions $\mathcal{F}_i(t,x)$, $\mathcal{V}_i^+(t,x)$ and $\mathcal{V}_i^-(t,x)$ are ω-periodic in t.
(A3) If $x_i = 0$, then $\mathcal{V}_i^- = 0$. In particular, if $x \in X_s$, then $\mathcal{V}_i^- = 0$ for $i = 1, \ldots, m$.
(A4) $\mathcal{F}_i(t,x) = 0$ for $i > m$.
(A5) If $x \in X_s$, then $\mathcal{F}_i(t,x) = \mathcal{V}_i^+(t,x) = 0$ for $i = 1, \ldots, m$.

Let $f = (f_1, \ldots, f_n)^T$, and define an $(n - m) \times (n - m)$ matrix

$$M(t)=\left(\frac{\partial f_i(t,x^0(t))}{\partial x_j}\right)_{m+1\le i,j\le n},\ F(t)=\left(\frac{\partial \mathcal{F}_i(t,x^0(t))}{\partial x_j}\right)_{1\le i,j\le n}\text{ and }V(t)=\left(\frac{\partial \mathcal{V}_i(t,x^0(t))}{\partial x_j}\right)_{1\le i,j\le n}.$$

(A6) We define $\Phi_M(t)$ as the monodromy matrix of the linear ω-periodic system $\frac{dz}{dt}=M(t)z$. We further assume that $x_0(t)$ is linearly asymptotically stable in the disease-free subspace X_s, that is, $\rho(\Phi_M(\omega))<1$, where $\rho(\Phi_M(\omega))$ is the spectral radius of $\Phi_M(\omega)$.

(A7) Let the $Y(t,s)$, $t\le s$, be the evolution operator of the linear ω-periodic system:

$$\frac{d}{dt}Y(t,s)=-V(t)Y(t,s),\quad \forall t\ge s,\quad Y(s,s)=I, \tag{28}$$

where I is the $m\times m$ identity matrix. we assume that $\rho(\Phi_{-V}(\omega))<1$.

Based on the assumptions above and setting by C_ω the ordered Banach space of all ω-periodic functions from $\mathbb{R}\times\mathbb{R}^m_+$, we can define a linear operator L: $C_\omega\to C_\omega$ by

$$(L\varphi)(t)=\int_0^\infty Y(t,t-a)F(t-a)\varphi(t-a)da,\quad \forall t\in\mathbb{R},\quad \varphi\in C_\omega. \tag{29}$$

The following theorem yields.

Theorem 4. *Let (A1)-(A7) hold. The basic reproduction number of system* (27) *defined as* $\mathcal{R}_0=\rho(L)$ *exists and the following statements are valid:*

(i) $\mathcal{R}_0=1$ *if and only if* $\rho(\Phi_{F-V}(\omega))=1$.
(ii) $\mathcal{R}_0>1$ *if and only if* $\rho(\Phi_{F-V}(\omega))>1$.
(iii) $\mathcal{R}_0<1$ *if and only if* $\rho(\Phi_{F-V}(\omega))<1$.

Thus, $x^0(t)$ *is asymptotically stable if* $\mathcal{R}_0<1$, *and unstable if* $\mathcal{R}_0>1$.

Computation of the monodromy matrix $\Phi_{-V}(t)$

The transformation of V is

$$\mathrm{V}=P.D.P^{-1}=\begin{pmatrix} A_1 & -\gamma_c\alpha\theta & 0 & 0 & 0\\ 0 & A_2 & 0 & 0 & 0\\ 0 & -\gamma(1-\theta) & A_3 & 0 & 0\\ -\xi_d & -\xi_c & -\xi_u & \mu_B & 0\\ -\gamma_d & -\theta(1-\alpha)\gamma_c & -\gamma_u & 0 & \mu+\sigma \end{pmatrix}$$

where

$$\mathrm{D}=\begin{pmatrix} A_1 & 0 & 0 & 0 & 0\\ 0 & A_2 & 0 & 0 & 0\\ 0 & 0 & A_3 & 0 & 0\\ 0 & 0 & 0 & \mu_B & 0\\ 0 & 0 & 0 & 0 & \mu+\sigma \end{pmatrix}\quad\text{and}\quad \mathrm{P}=\begin{pmatrix} -B_1 & -P_1 & 0 & 0 & 0\\ 0 & -P_2 & 0 & 0 & 0\\ 0 & -P_3 & -C_1 & 0 & 0\\ B_2 & P_4 & -C_2 & 1 & 0\\ B_3 & P_5 & C_3 & 0 & 1 \end{pmatrix}.$$

$$B_1 = \frac{b_1}{\sqrt{b_1^2+b_2^2+\gamma_d^2}}, \quad B_2 = \frac{b_2}{\sqrt{b_1^2+b_2^2+\gamma_d^2}}, \quad B_3 = \frac{\gamma_d}{\sqrt{b_1^2+b_2^2+\gamma_d^2}}$$

$$b_1 = A_1-\mu-\sigma, \quad b_2 = \frac{(A_1-\mu-\sigma)\xi_d}{A_1-\mu_B},$$

$$C_1 = \frac{d_1}{\sqrt{d_1^2+d_2^2+\gamma_u^2}}, \quad C_2 = \frac{d_2}{\sqrt{d_1^2+d_2^2+\gamma_u^2}}, \quad C_3 = \frac{r}{\sqrt{d_1^2+d_2^2+\gamma_u^2}},$$

$$d_1 = A_3-\mu-\sigma, \quad d_2 = \frac{(-A_3+\mu+\sigma)\xi_u}{A_3-\mu_B},$$

$$P_1 = \frac{\beta_1}{\sqrt{\beta_1^2+\beta_2^2+\beta_3^2+\beta_4^2+1}}, \quad P_2 = \frac{\beta_2}{\sqrt{\beta_1^2+\beta_2^2+\beta_3^2+\beta_4^2+1}} P_3 = \frac{\beta_3}{\sqrt{\beta_1^2+\beta_2^2+\beta_3^2+\beta_4^2+1}},$$

$$P_4 = \frac{\beta_4}{\sqrt{\beta_1^2+\beta_2^2+\beta_3^2+\beta_4^2+1}}, \quad P_5 = \frac{1}{\sqrt{\beta_1^2+\beta_2^2+\beta_3^2+\beta_4^2+1}}, \quad \beta_1 = \frac{(A_2-\mu-\sigma)(A_2-A_3)\alpha\gamma_c\theta}{\alpha_1},$$

$$\beta_2 = \frac{(A_1-A_2)(A_3-A_2)(-A_2+\mu+\sigma)}{\alpha_2}, \quad \beta_3 = \frac{(A_1-A_2)\alpha\theta\gamma_c(-A_2+\mu+\sigma)(1-\theta)}{\alpha_2},$$

$$\beta_4 = \frac{-\alpha\theta\gamma_c(-A_2+\mu+\sigma)\alpha_2\xi_d - (A_1-A_2)\alpha\theta\gamma_c(-A_2+\mu+\sigma)(-(A_3-A_2)(\gamma_d\xi_c-\gamma_c\xi_d)-\alpha\theta\gamma_c(1-\theta)(\gamma_d\xi_u-\gamma_u\xi_d))}{\gamma_c(A_2-\mu_B)\gamma_d\alpha_2},$$

$$\alpha_1 = -(\theta(1-\alpha)\gamma_c(A_2+A_1+A_3)+\theta(1-\alpha)\gamma_c(\gamma_u(1-\theta)+\gamma_d\theta))A_2 - A_1A_3\theta(1-\alpha)\gamma_c - A_1\theta\alpha\alpha\theta\gamma_c\gamma_u - A_3\alpha\theta\gamma_c\gamma_d\theta + A_1\alpha\theta\gamma_c\gamma_u\theta \quad \text{and}$$

$$\alpha_2 = -\alpha\theta\gamma_c(A_1\gamma_u - A_2\gamma_u)(1-\theta) - (A_3-A_2)(A_1\theta(1-\alpha)\gamma_c - A_2\theta(1-\alpha)\gamma_c + \alpha\theta\gamma_c\gamma_d\theta).$$

$$P^{-1} = \begin{pmatrix} -\frac{1}{B_1} & \frac{P_1}{B_1P_2} & 0 & 0 & 0 \\ 0 & -\frac{1}{P_2} & 0 & 0 & 0 \\ 0 & \frac{P_3}{P_2C_1} & -\frac{1}{C_1} & 0 & 0 \\ \frac{B_2}{B_1} & -\frac{B_2P_1C_1 - B_1P_4C_1 - B_1P_3C_2}{B_1P_2C_1} & -\frac{C_2}{C_1} & 1 & 0 \\ \frac{B_3}{B_1} & -\frac{B_3P_1C_1 - B_1P_5C_1 + B_1P_3C_3}{B_1P_2C_1} & \frac{C_3}{C_1} & 0 & 1 \end{pmatrix}$$

Since that each coefficient of matrix $V(t)$ isn't time varying on t, the resolution of the differential equation in Eq. (28) gives that

$$Y(t,s) = Y(s,s)\exp(-(t-s)V(t)) = \exp(-(t-s)V), \quad \forall t > s \geq 0.$$

A simple computation give that the modronomy matrix

$$\begin{aligned} \Phi_{-V}(t) &= \exp(-(t-s)V) \\ &= P\exp(-(t-s)D)P^{-1} \end{aligned} \tag{30}$$

$$= \begin{pmatrix} e^{-(t-s)A_1} & \frac{P_1}{P_2}(e^{-(t-s)A_2} - e^{-(t-s)A_1}) & 0 & 0 & 0 \\ 0 & e^{-(t-s)A_2} & 0 & 0 & 0 \\ 0 & \frac{P_3}{P_2}(e^{-(t-s)A_2} - e^{-(t-s)A_3}) & e^{-(t-s)A_3} & 0 & 0 \\ \frac{B_2}{B_1}(e^{-(t-s)\mu_B} - e^{-(t-s)A_1}) & \Phi_1(t) & \frac{C_2}{C_1}(e^{-(t-s)A_3} - e^{-(t-s)\mu_B}) & e^{-(t-s)\mu_B} & 0 \\ \frac{B_3}{B_1}(e^{-(t-s)(\mu+\sigma)} - e^{-(t-s)A_1}) & \Phi_1(t) & \frac{C_3}{C_1}(e^{-(t-s)(\mu+\sigma)} - e^{-(t-s)A_3}) & 0 & e^{-(t-s)(\mu+\sigma)}, \end{pmatrix}$$

where.

$\Phi_1(t) = \frac{P_1B_2}{P_2B_1}e^{-(t-s)A_1} - \frac{P_4}{P_2}e^{-(t-s)A_2} - \frac{P_3C_2}{P_2C_1}e^{-(t-s)A_3} - \frac{B_2P_1C_1 - B_1P_4C_1 - B_1P_3C_2}{B_1P_2C_1}e^{-(t-s)\mu_B}$ and $\Phi_2(t) = \frac{P_1B_3}{P_2B_1}e^{-(t-s)A_1} - \frac{P_5}{P_2}e^{-(t-s)A_2} + \frac{P_3C_3}{P_2C_1}e^{-(t-s)A_3} - \frac{B_3P_1C_1 - B_1P_5C_1 + B_1P_3C_3}{B_1P_2C_1}e^{-(t-s)(\mu+\sigma)}$.□

Computation of the basic reproduction numbers of systems (12) and (13)

Now, we compute the basic reproduction number. The disease free equilibrium *DFE* X^0 for system (3) is

$$X^0 = \left(\frac{\Lambda}{\mu}, 0, 0, 0, 0, 0\right)^T.$$

The basic reproduction numbers of systems (12) and (13) can be deduce directly from the basic reproduction number of system (3) when all parameters are constants. However, the basic reproduction number of system (3) with constant transmission rates (β_H and β_B) assumes the results of Van Den Driessche and Watmough (Van den Driessche & Watmough, 2002). One has that

$$\mathcal{F}_1(t) = \begin{pmatrix} \rho\delta\lambda(t)S(t) \\ \rho(1-\delta)\lambda(t)S(t) \\ (1-\rho)\lambda(t)S(t) \\ 0 \end{pmatrix} \quad \text{and} \quad \mathcal{V}_1 = \begin{pmatrix} -\theta\alpha\gamma_c C + (\gamma_d + d_d + \mu)I_d(t) \\ (\gamma_c + \mu)C(t) \\ -(1-\theta)\gamma_c C + (\gamma_u + d_u + \mu)I_u(t) \\ -\xi_d I_d(t) - \xi_c C(t) - \xi_u I_u(t) + \mu_B B(t) \end{pmatrix}$$

represent the vectors of new infections and the remaining transfer terms, respectively. Their Jacobian matrices evaluated at the *DFE* X^0 are

$$F_1 = \begin{bmatrix} \rho\delta\epsilon_1\epsilon_2\beta_H & \rho\delta\beta_H & \rho\delta\epsilon_1\beta_H & \rho\delta\dfrac{\beta_B\Lambda}{K\mu} \\ \rho(1-\delta)\epsilon_1\epsilon_2\beta_H & \rho(1-\delta)\beta_H & \rho(1-\delta)\epsilon_1\beta_H & \rho(1-\delta)\dfrac{\beta_B\Lambda}{K\mu} \\ (1-\rho)\epsilon_1\epsilon_2\beta_H & (1-\rho)\beta_H & (1-\rho)\epsilon_1\beta_H & (1-\rho)\dfrac{\beta_B\Lambda}{K\mu} \\ 0 & 0 & 0 & 0 \end{bmatrix}$$

and

$$V_1 = \begin{bmatrix} \gamma_d + d_d + \mu & -\theta\alpha\gamma_c & 0 & 0 \\ 0 & \gamma_c + \mu & 0 & 0 \\ 0 & -(1-\theta)\gamma_c & \gamma_u + d_u + \mu & 0 \\ -\xi_d & -\xi_c & -\xi_u & \mu_B \end{bmatrix}.$$

The inverse of V is

$$V_1^{-1} = \begin{bmatrix} \dfrac{1}{A_1} & \dfrac{\theta\alpha\gamma_c}{A_1A_2} & 0 & 0 \\ 0 & \dfrac{1}{A_2} & 0 & 0 \\ 0 & \dfrac{(1-\theta)\gamma_c}{A_2A_3} & \dfrac{1}{A_3} & 0 \\ \dfrac{\xi_d}{A_1\mu_B} & \dfrac{1}{A_2\mu_B}\left(\dfrac{\theta\alpha\gamma_c\xi_d}{A_1} + \xi_c + \dfrac{(1-\theta)\gamma_c\xi_u}{A_3}\right) & \dfrac{\xi_u}{A_3\mu_B} & \dfrac{1}{\mu_B} \end{bmatrix},$$

where

$$A_1 = \gamma_d + d_d + \mu,\ A_2 = \gamma_c + \mu \text{ and } A_3 = \gamma_u + d_u + \mu.$$

Then, the basic reproduction number of system (3) is the maximum eigenvalue of the next generation matrix $(F_1V_1)^{-1}$ given by

$$\mathcal{R}_0 = \mathcal{R}_{0d} + \mathcal{R}_{0C} + \mathcal{R}_{0u} + \mathcal{R}_{0B}. \tag{31}$$

$$\mathcal{R}_{0d} = \frac{\epsilon_1\epsilon_2\rho\beta_H}{A_1}\left(\delta + \frac{(1-\delta)\theta\alpha\gamma_c}{A_2}\right), \quad \mathcal{R}_{0C} = \frac{\rho(1-\delta)\beta_H}{A_2},$$

$$\mathcal{R}_{0u} = \frac{\epsilon_1\beta_H}{A_3}\left(1 - \rho + \frac{\rho(1-\delta)(1-\theta)\gamma_c}{A_2}\right) \quad \text{and}$$

$$\mathcal{R}_{0B} = \frac{\beta_B\Lambda}{K\mu_B\mu}\left[\left(\delta + \frac{(1-\delta)\theta\alpha\gamma_c}{A_2}\right)\frac{\rho\xi_d}{A_1} + \frac{\rho(1-\delta)\xi_c}{A_2} + \left(1 - \rho + \frac{\rho(1-\delta)(1-\theta)\gamma_c}{A_2}\right)\frac{\xi_u}{A_3}\right].$$

Finally, the computation of $\underline{\mathcal{R}_0}$ and $\overline{\mathcal{R}_0}$ can be deduce by substituting (β_H, β_B) by $(\beta_{hmin}, \beta_{bmin})$ and $(\beta_{hmax}, \beta_{bmax})$, respectively.□

Appendix C. States space formulation and *EnKf* approach

In this Appendix, we recall the formulation of *EnKf* approach (Bourgois et al., 2011) for the dual estimation of state variables and parameters.

EnKf for estimation of states and periodic parameters

Herein, our objective is to design an *EnKf* for the estimation both of state variables and parameters. We show how we can adapt *EnKf* to estimate periodic time-varying parameter. Note that, for the estimation problems, the formulation of *EnKf* is well known in the case that the estimated parameters are assumed to be constant (Guthke, Nowak, & Franssen, 2012; Yaqing & Dean, 2006). The new approach develop here is different to Arnold's method (Andrea & Alun, 2018) as that we consider that

it is the sinusoid coefficients which can change of one observation to another one. However, we use *EnKf* for an estimation using the periodicity and climatic changes of time-varying parameters. In this case, we consider the following system:

$$\begin{cases} x_{t+1} &= f(x_t, \psi_t) + w_t, \\ y_t &= h(x_t, \psi_t) + v_t, \\ \psi_{t+1} &= \psi_t + \chi_t, \end{cases} \tag{32}$$

where $x_t \in \mathbb{R}^n$ is the state variables given after discretization of the differential system. The observation that depend of the states and the parameters $\psi_t \in \mathbb{R}^l$ ($l \in \mathbb{N}$) is denoted by $y_t \in \mathbb{R}^m$ w_t and v_t are the white noises with the covariance matrices H_t and K_t, respectively. The estimation is done as follows.

1 Decomposition of periodic parameter (Andrea & Alun, 2018): we use the fact that ψ_t is periodic and estimate its at each time. For this, we consider ψ_t as time-varying parameters that involve with the time $t \in [0, T[$, where T is the period of these parameters. Also, we consider that in each period, the couple ψ_t have p values in each period as follows:

$$\psi^t = \begin{cases} \psi_1 & \text{if} \quad t = T/p, \\ \psi_2 & \text{if} \quad t = 2T/p, \\ \vdots & \\ \psi_p & \text{if} \quad t = T, \end{cases} \tag{33}$$

where p represents the number of observations during each period. Therefore, we need to estimate p values of ψ_t per period.

2 States space formulation of *EnKf*: Since each $(\psi_{0i}, \psi_{1i})_1^p$ are influenced by climate changes, we add white noises (Bourgois et al., 2011; Gillijns et al., 2006) so that the time-varying parameters ψ_{0i} and ψ_{1i} follow a Markov process as

$$\psi_i^{t+1} = \psi_i^t + \chi_i^t, \tag{34}$$

where χ_i^t represents the white noises with standard deviation and Q_i^t. The goal of this approach is to estimate each value of set $\{\psi_i^t\}_{i=1}^p$ using the following equations:

$$\begin{cases} x_{t+1} &= f(x_t, \psi_t) + w_t, \\ y_t &= h(x_t, \psi_t) + v_t, \\ \psi_{t+1} &= \psi_t + \chi_t, \quad \textit{if } t \in [0, T[, \\ \psi_t &= \psi_{t-kT} + \chi_t, \quad \textit{if } t \in [kT, (k+1)T[, \ k = 1, 2, \ldots, p-1. \end{cases} \tag{35}$$

For this, we will use the *EnKf* to estimate the sates and each ψ_t at time t giving in the next part of this Appendix. After having the estimation ψ_i^t, we use the last equation of (32) to have the estimation of ψ_t.

We apply this design of *EnKf* to fit epidemiological models using the seasonality in disease incidence and estimate the states and periodic time-varying rates.

EnKf Estimation Process with EnKf

Herein, we recall the *EnKf* approach (Bourgois et al., 2011) for estimating of state variables and parameters in the following system

$$\begin{cases} x_{t+1} &= f(x_t, \beta_t, u_t) + w_t, \\ y_t &= h(x_t, \beta_t) + v_t, \\ \beta_{t+1} &= \beta_t + \eta_t, \end{cases} \tag{36}$$

where $x_t \in \mathbb{R}^n$ is the state variables given after discretization of differential system. The observation that depends of the states and the parameters $\beta_t \in \mathbb{R}^p$ is denoted by $y_t \in \mathbb{R}^m$ w_t, v_t and η_t are the white noises with the covariance matrices Q_t, S_t and R_t, respectively. The estimation is done as that follows.

In the forecast step (see (Andrea & Alun, 2018; Gillijns et al., 2006; Kotecha & Djuric, 2003; Wan & van der Merwe, 2000)), we prepare both of the ensemble of n forecast states with random sampling error and the set of predicted outputs as

$$x_{t+1}^{fi} = f(x_t^{ai}, \beta_t^a, u_t) + w_t^i \quad \text{and} \quad y_{t+1}^{fi} = h(x_{t+1}^{fi}, \beta_t^a), \quad i = 1, 2, \ldots, n, \tag{37}$$

where the superscript *fi* refers to the *i*-th member of the ensemble of data, β_t^a is the estimate value of β_t at time t and the vector x_t^{ai} corresponds to the *i*-th member of the set of states corrected at the moment t. Then, for the step of correction, the sets means defined as follwos:

$$\overline{x}_{t+1}^f = \frac{1}{n}\sum_{i=1}^{n} x_{t+1}^{fi} \quad \text{and} \quad \overline{y}_{t+1}^f = \frac{1}{n}\sum_{i=1}^{n} y_{t+1}^{fi}. \tag{38}$$

are used to compute the covariance matrices of error at time $t + 1$ are

$$P_{xy,t+1} = \frac{1}{n-1}\sum_{i=1}^{n} E_{x,t+1}^{fi}\left(E_{y,t+1}^{fi}\right)^T \quad \text{and} \quad P_{yy,t+1} = \frac{1}{n-1}\sum_{i=1}^{n} E_{y,t+1}^{fi}\left(E_{y,t+1}^{fi}\right)^T, \tag{39}$$

where $E_{x,t+1}^{fi} = x_{t+1}^{fi} - \overline{x}_{t+1}^f$ and $E_{y,t+1}^{fi} = y_{t+1}^{fi} - \overline{y}_{t+1}^f$.

Thus, the forecast ensemble mean which is the best forecast estimate of the state, and the spread of the ensemble members around the mean as the error between the best estimate and the actual state by

$$R_{t+1} = \frac{1}{n-1}\sum_{i=1}^{n} v_{t+1}^i \left(v_{t+1}^i\right)^T. \tag{40}$$

The second step is to obtain the estimates analysis of the state.For this, the *EnKf* performs an ensemble of parallel data assimilation cycles. In this step, we update each available member of the set of draft states using the current observation and we each member of the following linear correction equation:

$$x_{t+1}^{ai} = \overline{x}_{t+1}^{fi} + K_{t+1}(y_{t+1} + v_{t+1}^i - y_{t+1}^{fi}),\ i = 1, 2, \ldots, n, \tag{41}$$

where

$$K_{t+1} = P_{xy,t+1}(P_{yy,t+1} + R_{t+1})^{-1} \tag{42}$$

is the gain of *EnKf*.

Herein, the estimate state of x_{t+1} at time $t + 1$ is given by:

$$x_{t+1}^a = \frac{1}{n}\sum_{i=1}^{n} x_{t+1}^{ai}. \tag{43}$$

The second design concerns the estimation β_{t+1}^a of the vector of parameters β_{t+1} at time $t + 1$.

As at the state estimation, we prepare the ensemble of N forecast states with random sampling error as

$$\beta_{t+1}^{fi} = \beta_t^{fi} + \eta_t^i,\ i = 1, 2, \ldots, n. \tag{44}$$

The ensemble mean is defined as

$$\overline{\beta}_{t+1}^f = \frac{1}{n}\sum_{i=1}^{n} \beta_{t+1}^{fi}. \tag{45}$$

The ensemble error matrix for the state variable is defined by

$$E_{\beta,t+1}^{fi} = \beta_{t+1}^{fi} - \overline{\beta}_{t+1}^f,\ i = 1, 2, \ldots, n. \tag{46}$$

and the ensemble error matrix for the observed variables is defined as follows:

$$E_{y,t+1}^{fi} = y_{t+1}^{\beta fi} - \overline{y}_{t+1}^{\beta f},\ i = 1, 2, \ldots, n, \tag{47}$$

where $y_{t+1}^{\beta fi} = h(x_{t+1}^{a}, \beta_{t+1}^{fi}) \quad i = 1, 2, \ldots, n$.For the analysis steps, the Kalman gain matrix of *EnKf* K_{t+1} is given by

$$K_{\beta,t+1} = P_{\beta y,t+1}(P_{\beta yy,t+1} + R_{t+1})^{-1}, \tag{48}$$

where the error covariance matrices $P_{\beta y,t+1}$ and $P_{\beta yy,t+1}$ are given by

$$P_{\beta y,t+1} = \frac{1}{n-1}\sum_{i=1}^{n} E_{\beta,t+1}^{fi}(E_{y,t+1}^{fi})^{T} \text{ and } P_{\beta yy,t+1} = \frac{1}{n-1}\sum_{i=1}^{n} E_{\beta yy,t+1}^{fi}(E_{yy,t+1}^{fi})^{T}. \tag{49}$$

References

Albalawi, W., Nisar, K. S., Aslam, A., Ozair, M., Hussain, T., Shoaib, M., et al. (2023). Mathematical modelling approach to cholera transmission with vaccination strategy. *Alexandria Engineering Journal, 75*, 191–207. https://doi.org/10.1016/j.aej.2023.05.053

Amber, P.. *The* 10 *worst epidemics in history*. https://www.worldatlas.com/articles/the-10-worst-epidemics-in-history.html.Wolrdfacts. (Accessed 23 August 2019). and visited 2016 Feb.

Andrea, A., & Alun, L. L. (2018). An approach to periodic, time-varying parameter estimation using nonlinear filtering. *Inverse Problems, 10*, Article 105005.

Appoh, E. A., Apraku, L. O., Agyei, W., & Denteh, W. O. (2015). *Modeling cholera Dynamics with a control Strategy in Ghana* British. *Journal of Research, 1*, 30–41.

Bacaër, N., & Gomes, M. G. M. (2009). On the final size of epidemics with seasonality. *Bulletin of Mathematical Biology, 1*, 1954–1966.

Bacaër, N., & Guernaoui, S. (2006). The epidemic threshold of vector-borne diseases with seasonality. *Journal of Mathematical Biology, 53*, 421–436.

Bourgois, L., Roussel, G., & Benjelloun, M. (2011). Kalman d'ensemble état-paramètres appliqué au modèle de Lorenz. https://www-lisic.univ-littoral.fr/publis/1323537933.pdf. (Accessed 5 August 2019).

Bowong, S., & Tewa, J. J. (2009). Mathematical analysis of a tuberculosis model with differential infectivity. *Communications in Nonlinear Science and Numerical Simulation, 11*, 4010–4021.

Brauer, F., Shuai, Z., & Driessche, P. V. D. (2013). Dynamics of an age-of-infection cholera model. *Mathematical Biosciences and Engineering, 10*, 1335–1349. https://doi.org/10.3934/mbe.2013.10.1335.shu

Burlando, L. (1991). Monotonicity of spectral radius for positive operators on ordered Banach spaces. *Archiv der Mathematik, 9*, 49–57.

Cazelles, B., Champagne, C., & Dureau, J. (2018). Accounting for non-stationarity in epidemiology by embedding time-varying parameters in stochastic models. *PLoS Computational Biology, 8*, 1–26.

CDC, Cholera - Vibrio Cholerae infection. Available on https://www.cdc.gov/Cholera/illness.html::text=Cholera.

Chao, D. L., Longini, I. M., & Morris, J. G. (2014). Modeling cholera outbreaks. *Current Topics in Microbiology and Immunology, 379*, 195–209.

Cholera platform, https://www.plateformeCholera.info/index.php/.

Chowell, G., & Brauer, F. (2009). *Mathematical and statistical estimation approaches in epidemiology*. Dordrecht: Springer. http://site.ebrary.com/id/10310274.

Conde, A., Dureh, N., & Ueranantasun, A. (2023). Trends and patterns of cholera epidemic in West Africa: A statistical modeling study. *Journal of Water and Health, 2*, 261–270. https://doi.org/10.2166/wh.2023.241

Deen, J., A Mengel, M., & Clemens, J. D. (2020). Epidemiology of cholera. *Vaccine, 38*, 31–40.

Diekmann, O., Heesterbeek, J. A. P., & Metz, J. A. J. (1990). On the definition and the computation of the basic reproduction ratio R0 in the models for infectious disease in heterogeneous populations. *Journal of Mathematical Biology, 28*, 365–382.

Dietz, K. (1976). The incidence of infectious diseases under the influence of seasonal fluctuations. *Mathematical Models in Medicine, 11*, 1–15.

Dumont, Y., & Thuilliez, J. (2016). *Human behaviors: A threat to mosquito control? Mathematical biosciences* (Vol. 281, pp. 9–23).

Eisenberg, M. C., Kujbida, G., Tuite, A. R., Fisman, D. N., & Tien, J. H. (2013). *Examining rainfall and cholera dynamics in Haiti using statistical and dynamic modeling approaches* (Vol. 5, pp. 197–207). Elsevier-Epidemics.

Fung, I. (2014). Chun-Hai, *Cholera transmission dynamic models for public health practitioners*. *Emerging Themes in Epidemiology, 11*. https://doi.org/10.1186/1742-7622-11-1

Gillijns, S., Barrero Mendoza, O., Chandrasekar, J., De Moor, B. L. R., Bernstein, D. S., & Ridley, A. (2006). What is the ensemble kalman filter and how well does it work?. In *Proceedings of the 2006 American control conference* (Vol. 1, pp. 14–16).

Guthke, A., Nowak, W., & Franssen, H. H.-J. (2012). Parameter estimation by ensemble Kalman filters with transformed data: Approach and application to hydraulic tomography. *Water Resources Research, 1*.

Hameni Nkwayep, C., Bowong, S., Tewa, J. J., & Kurths, J. (2020). Short-term forecasts of the COVID-19 pandemic: A study case of Cameroon. *Chaos, Solitons & Fractals, 140*, Article 110106.

Isaac, C.-H. F. (2014). Cholera transmission dynamic models for public health practitioners. *Emerging Themes in Epidemiology, 1*. https://doi.org/10.1186/1742-7622-11-1

Julier, S. J., & Uhlmann, J. K. (1997). A new extension of the Kalman filter to nonlinear systems. In *Proceedings of the SPIE 11th international symposium on aerospace/defense sensing*. Orlando: Simulation and Controls. Floride, USA.

King, A. A., Ionides, E. L., Pascual, M., & Bouma, M. J. (2008). Inapparent infections and cholera dynamics. *Nature, 454*, 877–880. https://doi.org/10.1038/nature07084

Kolaye, G., Damakoa, I., Bowong, S., Houe, R., & Békollé, D. (2018). Theoretical assessment of the impact of climatic factors in a Vibrio cholerae model. *Acta Biotheoretica, 4*, 279–291.

Kolaye, G., Damakoa, I., Bowong, S., Houe, R., & Békollè, D. (2020). A mathematical model of cholera in a periodic environment with control actions. *International Journal of Biomathematics, 13*. https://doi.org/10.1142/S1793524520500254

Kotecha, J. H., & Djuric, P. M. (2003). Gaussian particle filtering. *IEEE Transactions on Signal Processing, 51*, 2592–2601.

London, W. P., & Yorke, J. A. (1973). Recurrent outbreaks of measles, chickenpox and mumps: I. Seasonal variation in contact rates. *American Journal of Epidemiology, 98*, 453–468.

Marek, I. (1970). *Frobenius theory of positive operators: Comparison theorems and applications* (Vol. 3, pp. 607–628). Society for Industrial and Applied Mathematics.

Ministry of public health, Cholera Situation Reports. Available on https://www.ccousp.cm/documentations/rapports-de-situation-Cholera/..

Ministry of public health. (2018). *Cameroon: Cholera outbreak*. https://reliefweb.int/disaster/ep-2018-000142-cmr.

D. A. Montero, R. M. Vidal, J. Velasco, S. George, Y. Lucero, L. A. Gómez, L. J. Carreño, R. García-Betancourt, M. O'Ryan Vibrio cholerae, classification, pathogenesis, immune response, and trends in vaccine development. Frontiers of Medicine, 10, 1155751. https://doi.org/10.3389/fmed.2023.1155751.

Mukandavire, Z., Liao, S., Wang, J., Gaff, H., Smith, D. L., & Morris, J. G. (2011). Estimating the reproductive numbers for the 2008-2009 cholera outbreaks in Zimbabwe. *Proceedings of the National Academy of Sciences of the United States of America, 21*, 8767–8772.

Narula, P., Piratla, P., Bansal, A., Azad, S., & Lio, P. (2016). Parameter estimation of tuberculosis transmission model using Ensemble Kalman filter across Indian states and union territories. *Infection, Disease & Health, 21*, 184–191.

Nkwayep, C. H., Bah, A., Tsanou, B., & Bowong, S. (2023). *Mathematical modelling and forecasting of COVID-19 in Cameroon and Senegal*. Preprint.

Nkwayep, C. H., Bowong, S., Tsanou, B., Alaoui, M. A. A., & Kurths, J. (2022). Mathematical modeling of COVID-19 pandemic in the context of sub-Saharan Africa: A short-term forecasting in Cameroon and Gabon. *Mathematical Medicine and Biology: A Journal of the IMA, 1*, 1–48.
Phan, T. A., Tian, J. P., & Wang, B. (2021). Dynamics of cholera epidemic models in fluctuating environments. *Stochastics and Dynamics, 2*, Article 2150011. https://doi.org/10.1142/s0219493721500118
Phelps, M., Perner, M. L., E Pitzer, V., Andreasen, V., M Jensen, P. K., & Simonsen, L. (2018). Cholera epidemics of the past offer new insights into an old enemy. *The Journal of Infectious Diseases, 4*, 641–649.
Signing, F., Tsanou, B., Bowong, S., & Lubuma, J. (2010). Modelling and mathematical analysis the effects of periodic emission of aerosols on the dynamics of NmA. *Mathematics and Computers in Simulation*.
Stephen, E., & Nkuba, N. (2015). A mathematical model for the dynamics of cholera with control measures. *Applied and Computational Mathematics, 2*, 53–63. https://doi.org/10.11648/j.acm.20150402.14
Tan, Y., Cator, D., III, Ndeffo-Mbah, M., & Braga-Neto, U. (2021). A stochastic metapopulation state-space approach to modeling and estimating COVID-19 spread. *Mathematical Biosciences and Engineering, 18*, 7685–7710.
Tian, J. P., Liao, S., & Wang, J. (2021). Analyzing the infection dynamics and control strategies of cholera. *Stochastics and Dynamics, 2*, Article 2150011. https://doi.org/10.1142/s0219493721500118
UNICEF, Cholera Epidemiology and Response Factsheet Cameroon. Updated on March 2015 and visited on April 2023. https://reliefweb.int/report/cameroon/cholera-epidemiology-and-response-factsheet-cameroon..
Van den Driessche, P., & Watmough, J. (2002). Reproduction numbers and sub-threshold endemic equilibria for the compartmental models of disease transmission. *Mathematical Biosciences and Engineering, 180*, 29–48.
Wan, E. A., & van der Merwe, R. (2000). The unscented Kalman filter for nonlinear estimation. *Proc. The IEEE AS-SPCC Symposium*.
Wang, W., & Zhao, X.-Q. (2008). Threshold dynamics for compartmental epidemic models in periodic environments. *Journal of Dynamics and Differential Equations, 20*, 699–717.
WHO, Health data overview for the Republic of Cameroon: Leading causes of death. Available on https://data.who.int/countries/120.
WHO, *Global Health Observatory*: Cause-specific mortality, 2000-2019 Available on https://www.who.int/data/gho/data/themes/mortality-and-global-health-estimates/ghe-leading-causes-of-death.
WHO, Cholera ? Global situation. Available on https://www.who.int/emergencies/disease-outbreak-news/item/2022-DON426..
WHO, L'OMS situe la cause qui attise l'explosion du choléra dans le monde. Available on https://lalgerieaujourdhui.dz/loms-situe-la-cause-qui-attise-lexplosion-du-Cholera-dans-le-monde/..
WHO. (2018). *Weekly epidemiological record. No 38* (Vol. 93, pp. 489–500). and available on https://apps.who.int/iris/bitstream/handle/10665/274654/WER9338.pdf?sequence=5&isAllowed=y.
WHO AFRO. (2018). *Outbreaks and other emergencies*. Week 32: 4-10 August; *Data as reported by 17*:00.
WHO AFRO. (2019). *Outbreaks and other emergencies, week 4: 18-25 january 2019. Data as reported by 17:00*.
WHO Cholera. Available on https://www.who.int/news-room/fact-sheets/detail/Cholera.
Yaqing, G., & Dean, S. O. (2006). The ensemble Kalman filter for continuous updating of reservoir simulation models. *Journal of Energy Resources Technology, 1*, 79–87.